الجمهورية الجزائرية الديمقراطية الشعبي

PEOPLE'S DEMOCRATIC REPUBLIC OF ALGERIA

وزارة التعليم العالي والبحث العلمي

MINISTRY OF HIGH EDUCATION AND SCENTIFIC RESEARCH

University Saad Dahlab Blida 1

Institute of Aeronautics and Space studies

Department of Aeronautical Construction

Thesis

submitted for obtaining the degree of

Master in Aeronautics

Option : Aeronautical Structures

Theme :

Characterization of an Aluminum based metal matrix nanocomposites reinforced with Carbon Nanotubes(CNTs) and Boron Carbide(B₄C) processed by mechanical alloying

Supervisor : Hamlati Zineb   Presented by : Boussaa Thinhinane

Co-supervisor : Hachache Hacene   Chaib Akram

July 2023

Acknowledgements

I would like to express my gratitude to Dr. Hamlati Zineb for guiding me in this thesis and for her constructive remarks. Her unwavering support and encouragement have been invaluable.

I would also like to give special thanks to Dr. Hachache Hacene for his availability and insightful discussions throughout the thesis. His expert advice has been greatly appreciated.

We are thankful for the precious friendship and help of many colleagues,

Finally, we want to acknowledge the support of our families, who have been our silent partners in this work.

Dedication

It brings me great joy to dedicate this work to my beloved parent, my father, who has been a constant source of strength and guidance. He tirelessly worked to provide me with everything I needed and never expected anything in return. And for my dear mother, who also deserves recognition for her loving care and support.

I would also like to dedicate this work to my dear sisters Fatima, Anissa, and Maissa, for their unwavering encouragement and support. And also, for my brother Amayas who holds a special place in my heart, as he always goes above and beyond to meet my needs.

Lastly, this work is dedicated to all my friends, near and far, who have supported me on my journey. It is an honor to share this work with you all.

Sincerely,

Thinhinane

Dedication

This thesis is dedicated to my parents for their endless love, support, and encouragement .My sweet sisters Marwa and Amani and also my cousin Hemza.

And without forgetting my amazing partner for her perseverance, kindness, and hard work.

Sincerely,

Akram

Abstract

Multi-wall carbon nanotubes (MWCNTs), and boron carbide(B4C), have been successfully employed in the development of a nanocomposite based on an aluminum matrix by mechanical alloying using a Planetary Micro Mill Pulverisette 7. The milling is done for identical weight specimens at different processing times of (15,30 and 60 minutes).

The resulting powders are then consolidated by cold pressure. The mechanical properties were studied for the three specimens as a function of alloying time, using Scanning Electron Microscopy(SEM), X-Ray diffraction (XRD), and Nanoindentation.

The results show the effect of the milling time increase on the powders' mechanical properties.

Key words : Nanocomposites, Metal Matrix, Carbon nanotubes, Boron carbide, Mechanical Alloying, Scanning electron microscopy, X-ray diffraction, Nanoindentation.

Résumé

Les nanotubes de carbone multi-parois (MWCNT) et le carbure de bore (B4C) ont été utilisés avec succès dans le développement d'un Nanocomposites basé sur une matrice d'aluminium, par mécanosynthèse. le broyage planétaire a été effectué avec un (Planetary Micro Mill Pulverisette 7) pour des échantillons de masse identique à des durées de broyage différentes (15,30 et 60 minutes). Les poudres obtenues sont ensuite consolidées par pression à froid.

Les propriétés mécaniques ont été étudiées pour les trois échantillons en fonction du temps de broyage, à l'aide de la microscopie électronique à balayage (MEB), de la diffraction des rayons X (DRX) et de la nanoindentation.

Les résultats montrent l'effet de l'augmentation du temps de broyage sur les propriétés mécaniques des poudres.

Mots clés : Nanocomposites, matrice métallique, nanotubes de carbone, carbure de bore, mécanosynthèse, microscopie électronique à balayage, diffraction des rayons X, nanoindentation.

ملخص

يتكون العمل المقدم في هذه الأطروحة من تطوير مركب نانوي على أساس مصفوفة من الألومنيوم معززة بأنابيب الكربون النانوية (CNTs) وكربيد البورون (B$_4$C)عن طريق الطحن الميكانيكي باستخدام مطحنة الكوكبية الدقيقة Planetary Micro Mill Pulverisette 7 ، حسب أوقات المعالجة التالية (15 و30 و60 دقيقة). يتم بعد ذلك دمج المساحيق الناتجة عن طريق الضغط البارد.

تمت دراسة الخواص الميكانيكية للعينات الثلاث كدالة لوقت الطحن باستخدام المسح المجهري الإلكتروني (SEM) ، حيود الأشعة السينية (XRD) واختبار الصلابة الدقيقة (Nanoindentation) .

تظهر النتائج تأثير زيادة وقت الطحن على الخواص الميكانيكية للمساحيق.

كلمات مفتاحية: المركبات النانوية، المصفوفة المعدنية، الأنابيب النانوية الكربونية، كربيد البورون، الطحن الميكانيكي، الفحص المجهري للإلكترون ، حيود الأشعة السينية ، واختبار الصلابة الدقيقة.

Table of content

Table of illustrations

List of tables

General introduction

The aerospace industry has an increasing need for lightweight structural materials due to rising fossil fuel costs, the need to reduce carbon dioxide emissions and to prevent fatigue and corrosion issues. As a result, many aerospace companies have switched to using composite materials for structural components and the Boeing Dreamliner serves as a prime example of this technological development. This approach helps to reduce weight, fuel consumption, and emissions while still using high-strength materials.

Metal matrix composites (MMCs) stand out with their superior mechanical, thermal, and electrical properties. MMC have metal matrix, including aluminum, magnesium, copper, titanium, iron…Etc. They are reinforced with different materials, including metals, non-metals, and organic compounds to enhance properties such as stiffness, specific strength, wear resistance, and corrosion resistance. Since the late 19th century, aluminum alloys have been a popular and cost-effective choice for various uses. Beside to their recyclability, they are versatile and easily fabricated using traditional metalworking, forming, and joining techniques.

Owing to micro-composites' success, Nanocomposites are becoming increasingly popular, especially with advancements in nanotechnology. Aluminum matrix materials with nano-reinforcements are a variable option to address the limitations of aluminum (micro-) composites. These materials offer improved tensile strength, hardness, fracture toughness, and physical and thermal stability.

One dimensional Carbon nanotubes and metals-carbides are a popular choice for nano reinforcements due to their unique structure, which provides high aspect ratios, exceptional mechanical strength, and superior electrical and thermal conductivities, adding a small amount of carbon nanotube, and boron carbide to metals results in functional nanocomposites with unique mechanical and physical properties. As a result, both nano-reinforcements have received significant attention in the last decade for their outstanding performance. However, Manufacturing nanocomposites can be challenging as it involves properly dispersing particles and establishing strong bonds. Meeting these requirements is crucial for the material to perform well in extreme conditions.
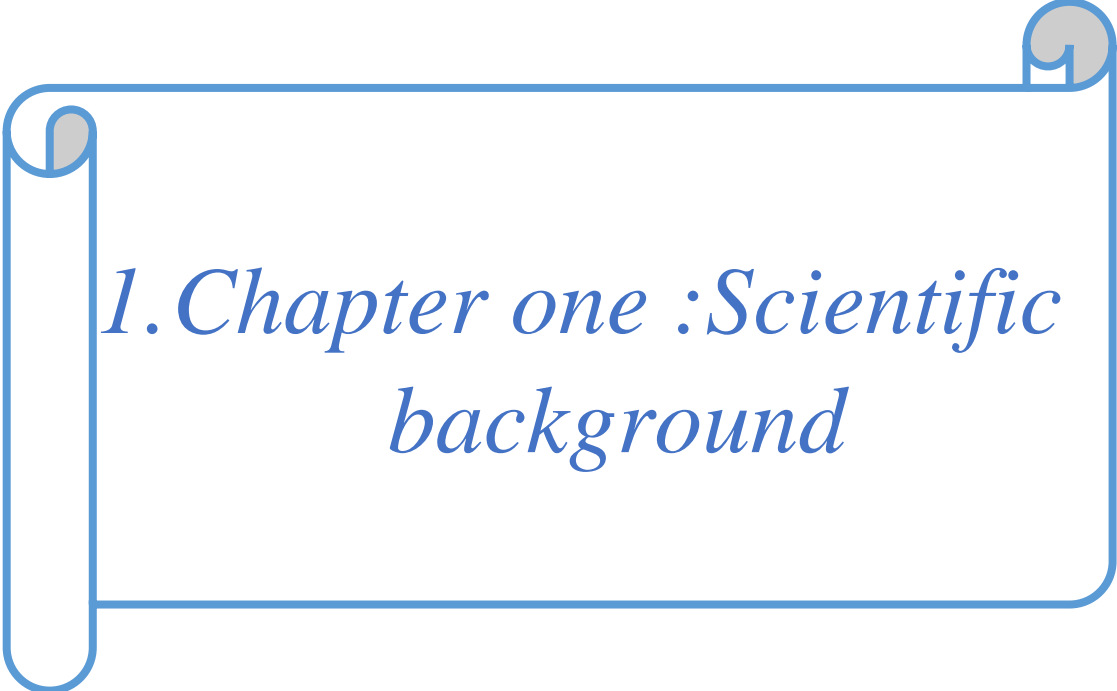
The goal of this study is to create nanocomposites using Mechanical Alloying at different processing time. The nanocomposites will comprise an aluminum matrix reinforced with Carbon Nanotubes (CNTs) and Boron Carbide (B_4C) in a fixed weight ratio of 0.2%.

In addition, a chemical agent was added to achieve this. The final chapter of the report presents a detailed analysis of the characteristics of the nanocomposites.

This thesis is divided into three chapters. The first chapter gives an overview of metal matrix nanocomposites and their use in the aerospace industry, particularly those based on aluminum. Then, it covers the main points of Carbon Nanotubes and Boron Carbide.

Chapter two delves into the development routes of nanocomposites, specifically emphasizing mechanical alloying. It then proceeds to present the elaboration of the (AL-2w%MWCNTs-2w%B$_4$C) nanocomposite with a Planetary Ball Milling.

The third chapter includes the analysis of collected specimens at different processing times, conducted through X-ray diffractometry, Scanning Electron Microscopy, and Nanoindentation. A general overview about the obtained result will be presented following each characterization method. Lastly, a conclusion of the work will be provided.

1.Chapter one :Scientific background

1.1 Introduction

In recent years, the aerospace industry has made significant progress in developing lightweight materials with superior mechanical and functional properties. Nanocomposites, made up of a matrix reinforced with nanoscale fillers and particles, are becoming increasingly popular in aerospace applications due to their ability to meet demanding requirements. Nanocomposites can enhance strength, stiffness, thermal stability, and other critical properties by adding nanoparticles to the matrix.

In the aerospace industry, materials need to be both strong and lightweight, as well as resistant to wear, corrosion, and fatigue, and withstand high temperatures. While traditional metal alloys have been used to meet these requirements, new innovative materials like Metal Matrix Nanocomposites (MMNCs) have been developed. These materials use nanoscale reinforcements to enhance the mechanical and functional properties of the metal matrix material, making them a promising solution for aerospace applications. The carbon nanotube has been intensely studied for its remarkable physical, chemical, and thermodynamic characteristics, making it a special reinforcement.

Studies of CNTs-strengthened composite structures have mainly concentrated on polymer structures. The main explanation for this intense focus is likely because the processing of polymers does not commonly necessitate high temperatures, which usually have to be used for metal and ceramic constructs. There seem to be few studies about CNT-reinforced ceramic matrices compared to that polymer matrices, and even fewer concerning those of metal matrix components. It is nothing short of astonishing that most of the substances employed in modern architecture are metals; however, differently structured metal matrix composites with Carbon Nanotubes reinforcement have incredible advantages such as lowered weight, enhanced strength, small coefficient of thermal expansion, and outstanding thermal conductivity, resources which open an array of potential uses.

This chapter provides a comprehensive overview of the application of nanocomposites in the aeronautical industry, with a specific focus on metal matrix nanocomposites featuring aluminum matrices. The chapter delves into two specific reinforcements used in the aerospace industry: Carbon Nanotubes and Boron Carbide. A closer look is taken into the creation and development of Carbon Nanotubes, emphasizing Multi-Wall carbon nanotubes. Additionally, the chapter covers the atomic structures, properties, and aerospace applications of these nanotubes and Boron Carbides.

1.2 Composites in the Aerospace Industry

The aerospace industry is devoted to enhancing the capability of both military and commercial airplanes, occasionally sparking the formation of reinforced structural materials of higher value. Composite materials are utilized in various aerospace uses, having an outsized impact in present-day aviation. These items are highly sought after because they can yield much higher strength-to-weight ratios and advantageous characteristics for withstanding harsh conditions.

Composite materials contribute immensely to weight loss, so they are essential to the structural construction and pieces used in every craft, from airframes, flight control surfaces, fairings, empennage, main rotor hub, and blades to turbine engine fan blades[1].

In the past, composite materials were only used in secondary structures. However, as knowledge and materials have improved, their use in primary structures such as wings and fuselages has increased. In the past, only two percent of the structural weight of the F15 was composed of composites. However, the percentage has grown considerably in the F18 to 19 percent and in the F22 to 24 percent. The Eurofighter extensively uses composites, with 40 percent of its structural weight comprising carbon-fiber reinforced composite material. Toughened epoxy skins make up around 75 percent of the exterior area. Other European fighters typically feature between 20 and 25 percent composites by weight, with Dassault's Rafael at 26 percent and the Saab Gripen's EADS Mako at 20 to 25 percent.

Commercial transport aircraft can benefit from composite materials, as it reduces airframe weight and leads to better fuel economy, ultimately lowering operating costs. Airbus first implemented composite materials in their aircraft in 1983, starting with the rudder of A300 and A310, followed by the vertical tail fin in 1985. The composite fin required fewer parts than its metal counterpart, significantly reducing weight and production costs. Over time, Airbus utilized composite materials for various structures in A320, including the entire tail structure, fuselage belly skins, fairings, access panels, deflectors, flaps, spoilers, ailerons, wheel doors, main gear leg fairing doors, and nacelles. Additionally, the floor panels were made of GFRP. Overall, composites make up 28 percent of the A320 airframe's weight.

The A340-500 and 600 airplanes have incorporated composite structures in their design, including the rear pressure bulkhead, keel beam, and portions of the wing's fixed leading edge. This marks a significant milestone for commercial transport aircraft as it is the first time a thermoplastic matrix composite component has been utilized. Approximately 20-

22% of the A380 is composed of composites by weight, and GLARE (glass-fiber reinforced aluminum alloy) is also utilized in several parts. GLARE laminates are created by bonding four or more 0.38 mm (0.015 in) thick aluminum alloy sheets with glass fiber resin. Using composites has resulted in a 20 percent reduction in weight, lower production time, and improved damage tolerance. The A380's top and bottom skin panels' front, center, and rear spars contain CFRP, which is also utilized in the rear pressure bulkhead, upper deck floor beams, ailerons, spoilers, and outer flaps. Lastly, the belly fairing is comprised of roughly 100 composite honeycomb panels[2].

The Boeing 787 **(Figure1.1)** comprises nearly 50% composite materials, resulting in an average weight savings of 20%. This is the highest usage of composite materials in any previous Boeing commercial airplane. The design process was approached without preconceived ideas, allowing Boeing engineers to choose the best material for each application throughout the airframe. This resulted in an airframe composed of almost half carbon fiber reinforced plastic and other composites, saving an average of 20% in weight compared to traditional aluminum designs. Each area of the airframe was analyzed to determine the best material considering the operating environment and loads that each component would experience over the life of the airframe. For example, aluminum handles compression well but is sensitive to tension loads, while composites are the opposite. This analysis resulted in the increased use of titanium, a low-maintenance design solution that can withstand comparable loads better than aluminum and is highly corrosion-resistant. Roughly 14% of the total airframe is made up of titanium. Using composite materials in the primary structure promises to reduce airlines' scheduled and nonroutine maintenance burdens. Every structural element of the 787 has undergone this life-cycle analysis, and material types were selected through a thorough and disciplined process[3].
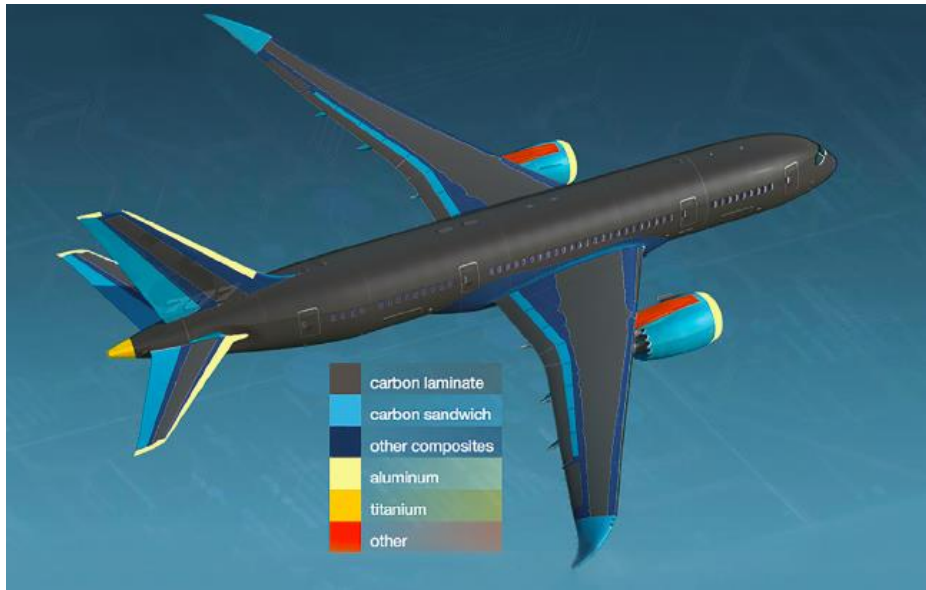
Figure 1.1 *composition of the Dreamliner 1 [4]*

In helicopters, there has been significant progress in creating various parts using materials like glass strands, carbon, or Kevlar fibers. Compared to non-rotary blade aircraft, rotary-winged planes increasingly rely on composite fabrics for construction. From the beginning, helicopter manufacturers have relied on this concept out of necessity. While weight is a crucial factor in fixed-wing design, it is even more crucial in helicopter design. This is because early helicopter engines were known for being underpowered[5]. All composite step procedure was first developed for use in military helicopter. The Airbus Helicopters-produced Tiger and NH90 **(Figure 1.2)** each composed of roughly 90 % CFRP, created as it meets the specific criteria of military execs, with particular priority given to vertical speed capabilities[6]. Benefitting from a modern approach to materials, the NH90's composite fuselage has fewer parts and a lower structural weight, resulting in 30% more endurance compared to a metallic fuselage, plus increased resistance to battle damage – among other benefits. The composite rotor blades have greater fatigue strength, damage tolerance and component lifetimes, as well as improved aerodynamic performances.

Figure 1.2 *NH90 NFH Nato Frigate Helicopter 1[7]*

1.3 Composites and Nanocomposites

Composite materials have significantly broadened the scope of available material properties, enhancing overall performance by combining the properties of their constituents. This is achieved by meticulously selecting materials to create superior property combinations. However, it may be necessary to make some compromises during the production of composites[8].

Composite materials are engineered from two or more entities (constituted of one matrix and one or more reinforcements) to create a new variant featuring increased traits. These items have become incredibly significant in different industries, encompassing air and space travel, automotive engineering, building projects, and athletics. Composites are materials made from polymers, ceramics, and metals matrices **(Figure 1.3)**. The most commonly used composites are polymer matrix composites, created by blending a polymer matrix with reinforcing fibers like carbon, glass, or aramid.

Composites with a high strength-to-weight ratio are commonly used in applications where reducing weight is crucial. Ceramic matrix composites pair a ceramic and a reinforcing constituent, such as silicon carbide or alumina, which are recognized for their heat-resistant qualities and remarkable performance at elevated temperatures. Metal matrix composites contain metals and/or ceramics as reinforcers, with a reputation for excellent tension aversion and stable stiffness even in heated conditions.
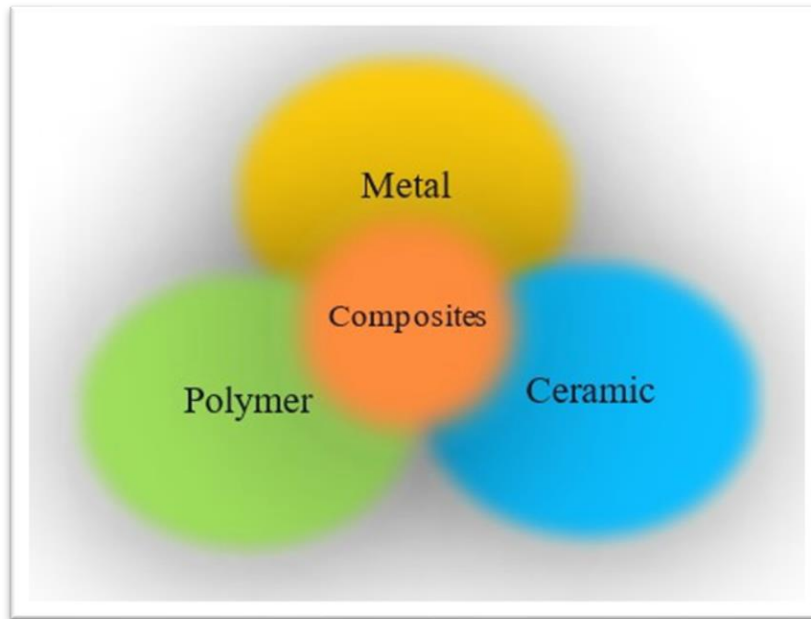
Figure 1.3 *Combination of Materials*

Composites come in different types with distinct properties and benefits, making them ideal for various applications. They have transformed how products are designed and made by providing enhanced performance, durability, and efficiency compared to conventional materials. However, Using micron-sized reinforcements in composites has limitations, such as reduced ductility and toughness compared to the matrix without reinforcements and excessive wear damage in tribological applications. Additionally, machining can cause highly high tool wear. Nanocomposites have been developed to address these issues and improve materials' tensile strength, hardness, and dimensional stability while maintaining good ductility and fracture toughness at both room and high temperatures. These composites use reinforcing phases that are less than 100 nanometers in size[9].

Nanocomposites are materials that are designed to exhibit superior performance properties by incorporating one or more nano reinforcing parts to the matrix[10]. Nano reinforcements are materials that have a size smaller than 100 nm in at least one characteristic dimension, like grain size, cylindrical cross-section diameter, or layer thickness. These materials can be metallic, polymeric, or ceramic; they can be categorized based on their geometry, which falls into three categories:

1) Nanoparticles are particles with dimensions in the nanometer range, also known as nanogranules or nanocrystals. They are equiaxed, meaning they have equal dimensions in all directions.

2) Nanotubes are elongated structures with two dimensions in the nanometer scale and one larger dimension. They are also called nanofibers, whiskers, or nanorods.

3) Nanolayers are tiny layers with a nanometer-scale dimension, sheets that are a few nanometers thick and hundreds to thousands of nanometers in length. They are also referred to as nanosheets, or nanoplatelets.

Nanocomposites have significantly better physical and mechanical properties compared to conventional micro-composites. The advantages of using nanoscale reinforcements instead of traditional fillers include a low-percolation threshold of around 0.1-2 vol.%, a high number density of particles per particle volume (ranging from 106-108 particles/μm^3), an extensive interfacial area per volume of particles (ranging from 103-104 m^2/ml), and short distances between particles (around 10-50nm at approximately 1-8 vol.%). While any material can be produced in a nanoscale shape and size, carbon nanotubes and boron carbide are one of the best choices commonly used[10].

1.4 Metal Matrix Nanocomposites

As the demand to lower fuel usage and emissions from ground support and aerospace vehicles rises, using light alloys to create structural components is becoming more common. Metals are widely used in engineering because they offer versatility and the ability to control their properties through alloy composition and processing methods. They are renowned for their strength, toughness, and cost-effectiveness. Nano reinforcements have been added to metals to create metal matrix nanocomposites (MMNCs), which enhance their properties. These MMNCs are highly beneficial for industrial applications requiring strong and lightweight structures.

Metal-matrix nanocomposites (MMNCs) are superior to their base metal equivalents in terms of high-temperature durability and the ability to enhance specific properties, such as stiffness, strength, abrasion resistance, creep resistance, thermal conductivity, and dimensional stability, due to the use of a ductile metal matrix. They outperform polymer-matrices in several ways, including their ability to withstand higher temperatures, processes a non-flammable nature, and a higher resistance to degradation by organic fluids. A wide range of metals, such as superalloys, aluminum, magnesium, titanium, and copper, are utilized as matrix nanomaterials.

There are several ways in which Metal matrix are different from other matrices. Firstly, the matrix phase of a MMNC is made up of a pure or alloy metal, unlike polymers or ceramics matrices in composites and nanocomposites. Secondly, MMNCs tend to have higher ductility and toughness levels than ceramics matrices. However, they need to match up to the ductility and toughness of their respective unreinforced metal matrix alloys. Thirdly, the nano reinforcement in MMNCs increases strength and modulus, similarly to Polymer Matrix Composites (PMCs), whereas, in Ceramic Matrix Composites (CMCs), the reinforcement is aimed at improving damage tolerance. Lastly, MMNCs can withstand higher temperatures better than polymers metrices[11].

1.4.1 Advantages and Limitations of a Metal Matrix Nanocomposites

Metal matrix Nanocomposites offer numerous benefits, including low coefficients of thermal expansion, lower creep rates, better fatigue resistance, high performance, durability, excellent strength-to-weight ratios, better wear resistance, and better radiation resistance. However, despite these advantages, they have limitations that must be considered, such as being challenging to machine, costly with limited supply, and potential for environmental degradation, as well as inconsistencies in material properties[12].

1.4.2 Types of Metal Matrices

MMCs and MMNCs are classified into different categories depending upon their matrix materials. Some examples of most commonly used metallic matrix configurations are(4):

• Aluminum-based composites; aluminum as matrix can be either cast alloy or wrought alloy (i.e., AlMgSi, AlMg, AlCuSiMn, AlZnMgCu, AlCu, AlSiCuMg).

• Magnesium-based composites

• Titanium-based composites

• Copper-based composites

• Super alloy-based composites

Aluminum is the most commonly used matrix material for MMCs in commercial applications, with various aluminum alloys available in various forms. Most aluminum

alloys have a similar density to pure aluminum, which makes them easy to process through solid-state methods like powder metallurgy or casting due to their relatively low melting temperature. Aluminum alloys can be classified as wrought or cast materials, with many wrought compositions available in powder form. Wrought aluminum alloys are mechanically worked into products like rolled sheets, plates, or foil, while cast aluminum alloys are available as ingots or other forms suitable for remelting. Aluminum alloys are frequently used to produce cast components using DRA (Discontinuously reinforced aluminum) with stirring to suspend particles in the liquid metal prior to casting and solidifying the article. Aluminum is also suitable for extrusion, making it a popular choice for most discontinuously reinforced aluminum MMCs[11].

1.4.3 Aluminum Metal Matrix Composites

The aluminum alloys have low density, good corrosion resistance, the capability to be strengthened by precipitation, high vibration damping capacity, and high thermal and electrical conductivity. Due to these properties, aluminum alloys are very favorable for metal matrix composites.

Aluminum matrix composites have been used since the 1920s. They can be used in a large area due to various mechanical properties. Aluminum is usually reinforced by aluminum oxide, silicon carbide, boron nitride, graphite, carbon nanotubes, boron carbide, etc. As a matter of fact, the addition of reinforcements to soft aluminum alloys can significantly improve the properties of the composite mainly when particles are in nano-scale. Recently, carbon nanotubes (CNTs) have attracted great interest in the scientific community as a new reinforcement material for producing novel aluminum MMCs.

1.4.4 Advantages and Limitations of an Aluminum Matrix

Aluminum Metal Matrices have a higher specific strength and stiffness than un-reinforced aluminum alloys. They also possess improved high-temperature creep and wear resistance. However, they are less ductile and tough.

Compared to ceramic matrix composites, aluminum matrix composites have higher toughness and ductility, are easier to elaborate, and are cost-effective. However, ceramics have high thermal resilience.

Compared to polymer matrix composites, aluminum matrix composites have higher transverse strength, toughness, better damage tolerance, environmental resistance, thermal and electrical conductivity, and temperature capability. Nevertheless, polymer matrix composites are more cost-effective[13].

1.5 Types and Role of Reinforcements

There are two main groups of reinforcements: particulates and fibers. Within fibers, there are two subcategories - continuous and discontinuous **(Figure 1.4)**. The fibers improve strength in the direction they are oriented. Continuous fiber-reinforced MMNCs have lower strength in the direction perpendicular to the fiber orientation, while discontinuously reinforced MMNCs display more isotropic characteristics. In some MMNC systems, two or more types of reinforcements may be used to impart specific properties.

In structural MMNCs, the role of the reinforcement varies based on its type. In particulate and whisker-reinforced MMNCs, the matrix bears most of the load. The reinforcement aims to enhance the composite's strength and stiffness by preventing matrix deformation through mechanical restraint, determined by the interparticle spacing to particle diameter ratio. In continuous fiber-reinforced MMCs, the reinforcement is the primary load-bearing component. The metallic matrix holds the reinforcing fibers together and distributes and transfers the load. Discontinuous fiber-reinforced MMCs exhibit properties between those of continuous fiber and particulate-reinforced composites. Adding reinforcement typically increases strength, stiffness, and temperature capability while decreasing the thermal expansion coefficient. The reinforcement also reduces the density of the composite when combined with a metallic matrix of higher density, resulting in enhanced specific strength[11].

a) Continuous fiber reinforcement
b) Discontinuous short fiber or whiskers reinforcement
c) Particle reinforcement

Figure 1.4*: Reinforcement types [14]*

a) Continuous Fiber Reinforcement

Primarily carbon (graphite) or ceramic are utilized in continuous fiber reinforcement. Ceramic types are alumina, silica, boron, zirconia, boron, nitride, and boron carbide. These types of filaments are weak, defective materials. Fewer materials are available in continuous fiber shape when compared with the particles. There are two types of fibers which are monofilament and multifilament. Either one of the fiber types is used in most of the composites.

b) Short Fiber / Whiskers Reinforcement

Short fibers stand in the middle between long fibers and particles concerned with the reinforcing and strengthening effect, whereas continuous fiber results in high anisotropic mechanical properties, and particle reinforcement results in nearly isotropic properties. Therefore, it is possible to vary the mechanical properties by using short fibers with the right amount and reinforcing fibers.

When it comes to whisker reinforcement, whiskers are tiny, needle-like single crystals with a diameter of 1μm. They are processed from oversaturated gases from solids or electrolysis solutions. Due to the production conditions, they contain low defect density. Their small size has led to a discussion about the health risks. They can be inhaled, leading to the carcinogenic effect.

c) Particle Reinforcement

Hard ceramic particles are generally chosen for the reinforcement of magnesium alloys. Particle materials are carbides (B_4C), nitrides (BN), oxides (Al2O3), and borides (WB). The chemical reactivity between the matrix and the particles is considered while

choosing the reinforcement type. An interface layer is essential for transferring the external and internal stresses to achieve good mechanical properties. The type and size of reinforcement influence the composite properties and the particles' shape. Three types of particle shapes are available: round, blocky, and platelet. Generally, platelet shape forms a good bonding contact with a crystal plane, which is impossible in round particles. Usually, sharp edge particles are not considered because the edges can act as a starting point for cracks when the material is loaded. For attaining a low-density composite, the reinforcement particle density should be low.

1.5.1 Main Reinforcements used to improve Aluminum Matrices

Oxides such as Al2O3, are commonly included to enhance metallic matrices' properties. These additives provide increased ductility and fracture toughness to the matrix, resistance to creep, and heightened strength.

Recent research has used *nitrides*, such as Si3N4 nanoparticles, to enhance mechanical properties. Additionally, there has been a focus on layered boron nitride, which has shown promising results. BN nanotubes incorporated in an Al matrix have demonstrated exceptional elastic modulus (ranging from 750 to 1200 GPa), strength (61 GPa), and chemical inertness (able to withstand oxidation up to 950 °C). These properties significantly enhance mechanical strength and thermal conductivity. However, the specific values achieved may vary depending on the processing technique.

Numerous researchers have studied various *carbides*, including SiC and WC, and B4C. Among these, SiC and B4C are frequently used reinforcements for MMNCs due to their exceptional properties such as high strength, low thermal expansion, high thermal conductivity, high hardness, high elastic modulus, high chemical inertness, and good wettability by the Al matrix.

Carbon nanotubes are commonly used to reinforce aluminum and its alloys, which are the most widely used non-ferrous structural materials. The initial report on the metal-CNT system was published in 1998 and focused on Al-CNT[9]. Carbon nanotubes (CNTs) are one of MMC's most widely researched strengthening additives. Their strong sp2 bonds contribute to their high elastic stretching properties. Multi-wall carbon nanotubes, in

particular, can reach a theoretical elastic modulus of 600 to 1100 GPa and tensile strength ranging from 35 to 110 GPa. Researchers Bakshi and Agarwal have reviewed the strengthening properties of CNT-Al composites, with record yield strength and elastic modulus of 621 MPa and 110 GPa, respectively[16]. In the following paragraphs, a summary of CNTs and B_4C will be provided.

1.6 Development of Carbon Nanotubes

1.6.1 History of Carbon Nanotubes

In 1991, Sumio Iijima was accredited as the one who identified carbon nanotubes. However, it is recognized that MWCNTs were, in reality, synthesized several decades before Iijima's paper[17]. Most notable are the filamentous tubes synthesized by Radushkevich et al. in 1952[18]. Researchers from the former USSR accomplished the work; its significance was not acknowledged in the first place because the term nanotechnology was just introduced in the 1970s, and the work was not read in the West simply because it was published in Russia[17]. Oberlin et al. in 1976 had produced hollow tubes of carbon ranging between 2 and 50 nm in diameter by decomposition of a mixture of benzene and hydrogen. They had described the structure as "turbostratic stacks of carbon layers, parallel to the fiber axis and arranged in concentric sheets like the annular rings of a tree."[18].

C60 was the first fullerene to be discovered in 1985 by Rick Smalley and coworkers. C60, or "buckyball," is a soccer ball (icosahedral), a shaped molecule with 60 carbon atoms bonded together in pentagons and hexagons. The carbon atoms are sp2 hybridized, but in contrast to graphite, they are not arranged on a plane. The geometry of C60 strains the bonds of the sp2 hybridized carbon atoms, creating new properties for C60. Graphite is a semimetal, whereas C60 is a semiconductor[19]. Following the discovery of C60, it was hypothesized that a tiny carbon fiber could be manufactured in which every new layer of graphene extended around the fiber and joined back up on itself. Potentially the thickness of this fiber could be just a single layer of graphene. These structures are the multi-walled carbon nanotube MWCNT and the single-walled carbon nanotube SWCNT[17]. Although carbon nanotubes might have been synthesized earlier, it took the genius of Iijima to realize that these were made up of multiple seamless tubes arranged in a concentric manner as opposed

to the scroll-like structure of filaments proposed by Bacon in 1960[18]. So, the synthesis of MWCNTs is widely credited to Iijima in 1991, a Japanese physicist; he found carbon fibers while working at NEC Corporation's fundamental research laboratory. Iijima observed a unique structure in a transmission electron microscope (TEM) image of graphite **(Figure 1.5)**, which appeared to be a cylindrical carbon molecule with a hollow interior. Subsequent to the discovery of multi-walled carbon nanotubes (referred to as CNT throughout the next chapters)[17], single-walled carbon nanotubes were discovered independently by Iijima and Ichihashi and Bethune et al. and reported in the same issue of Nature in 1993[18]. One of the most significant breakthroughs in the history of CNTs was the development of a technique for synthesizing them in large quantities in 1999 by researchers at Rice University. This technique called the arc discharge method, involved heating two graphite electrodes in a vacuum chamber and allowing the resulting carbon plasma to condense on a more excellent surface, forming CNTs. To fully understand and assimilate carbon nanotubes and to summarise some of the essential synthesis methods, including arc discharge, laser ablation, and chemical vapor decomposition (CVD), each of these will be expanded on in more details; in addition, the structure and electrical, mechanical, and physical properties and applications of CNTs will be discussed in the following paragraphs.
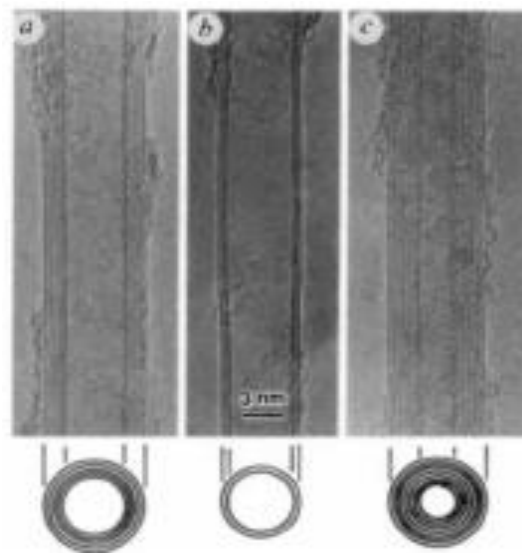
Figure 1.5 *TEM image of multiwalled carbon nanotubes [20].*

1.6.2 Carbon and Allotropes

Carbon is the most versatile element in the periodic table, owing to the type, strength, and number of bonds it can form with many different elements. In addition, the diversity of bonds and their corresponding geometries enable the existence of structural isomers, geometric isomers, and enantiomers. These are found in large, complex, and diverse structures, allowing for various organic molecules[19].

Carbon in the solid phase can exist in three allotropic forms: graphite, diamond, and fullerenes **(Figure 1.6)**, both graphite and diamond are giant covalent structures, meaning they are made of a regular lattice of covalently bonded atoms which makes them both strong. In a diamond, each carbon atom is covalently bonded to four other carbon atoms, the maximum number of bonds carbon can make and form a crystalline structure. The crystalline network gives the diamond its hardness with an extremely high melting point (the hardest substance known) and excellent heat conduction properties (about five times better than copper). However, it does not conduct electricity because it has no free electrons or ions that can move around. The sp3 hybridized bonds account for its electrically insulating property and optical transparency[19].

Graphite is made by layered planar sheets of sp2 hybridized carbon atoms bonded together in a hexagonal network. The different geometry of the chemical bonds makes graphite soft, slippery, opaque[19]; graphite still has a remarkably high melting point because the individual layers are strongly held together with covalent bonds. And since graphite has one spare electron that is not using in bonding this electron becomes delocalized which basically means that it is free to move around. And all these free electrons allow the graphite to conduct electricity and heat.

A single layer of graphite is known as graphene and scientist can actually isolate these individual layers and use them to make other structures such as spheres and tubes; we call these structures fullerenes. The tubular form of the fullerenes are carbon fibers and carbon nanotubes. The nanotubes will be the subject of the next section, and a detailed description of their synthesis, properties, and challenges will be given.

Carbon nanotubes (CNTs) are unique tubular carbon networks with a few nanometers diameter and a large aspect ratio. The nanotubes may consist of one to few tens of concentric carbons shells with adjacent shells separating ~0.34 nm. CNTs made

of one hollow seamless graphitic shell are called single-wall carbon nanotubes (SWCNTs) and typically have 0.6–3 nm diameters. CNTs of two or more seamless concentric shells are called multi-walled carbon nanotubes (MWCNT**s**)[21]. the curvature of the graphite flakes induced by rolling up to form the fibre is not sufficient to induce significant changes to the properties of the individual flakes[17]**,** and a single pristine layer of graphene does not extend all the way round the fibre; this distinguishes SWCNTs from MWCNTs.
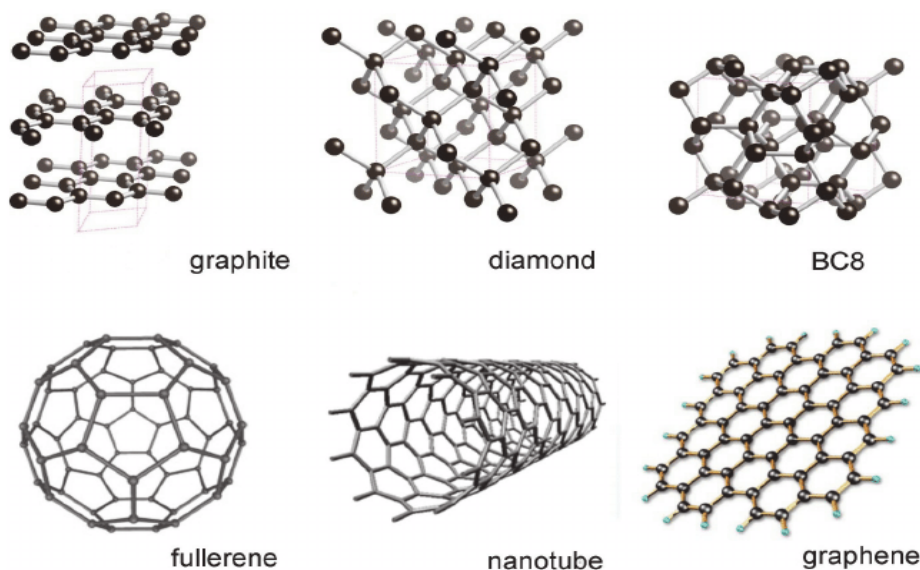
Figure 1.6 Carbon Allotropes [22]

1.6.3 Synthesis and Purification of Carbon Nanotubes

1.6.3.1   Synthesis of Carbon Nanotubes

Electric arc-discharge and laser ablation initially were the common approaches to nanotube synthesis. CNTs are now manufactured employing chemical vapor deposition (CVD) due to the new possibilities associated with that technology.

Arc discharge method **(Figure 1.7)** is the easiest and most commonly used method for producing CNTs in an inert gas at ~100 torr. In this method, when an electric arc discharge is generated between two graphite electrodes under inert atmosphere of helium or argon, a very high temperature of about 4000 K is obtained which allows the sublimation of the carbon from the anode[21]. Iijima produced the first MWCNTs by this method. He found

that nanotubes formed on the cathode, along with soot and fullerenes. For the growth of single-wall tubes, a metal catalyst is needed in the arc–discharge system.

The first success in producing substantial amounts of SWCNTs by arc discharge was achieved by Bethune and coworkers in 1993[23]. The anode–cathode distance can be changed to vary the strength of the plasma formed in between. The overall gas pressure has been shown to affect the weight percent yield of SWCNTs. Several metal catalyst compositions produce SWCNTs, but the current standard widely used for its production is a (Yttrium: Nickel) mixture that has been shown to yield up to 90% SWCNT, with an average diameter of 1.2 to 1.4 nm. In general, the nanotubes produced by this synthesis method need extensive purification before use. On the other hand, both SWCNTs and MWCNTs made from this process are now commercially available relatively inexpensively and have been for several years[19].
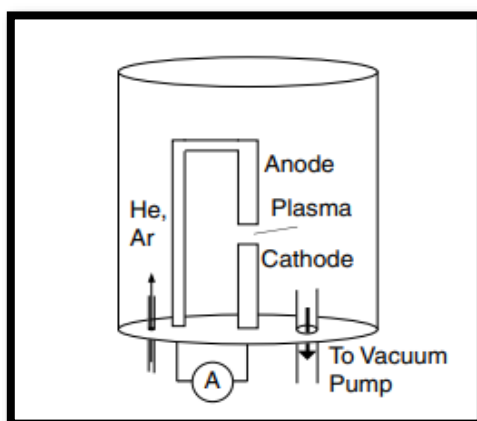
Figure 1.7 Arc Discharge Method [19].

Another method, laser ablation **(Figure 1.8),**was introduced to synthesize SWCNTs later on. This approach involves the laser ablation in a He atmosphere of a graphite target, which is impregnated with a transition metal catalyst. This method can be used to produce long bundles of single-wall carbon nanotubes. However, CVD, which is based on the decomposition of hydrocarbons such as acetylene or methane on catalytic particles (Fe, Cu, Co), is currently the most common method for the synthesis of carbon nanotubes, due to its capacity to produce variety of carbon nanotubes and industrial upscaling[18]**.**
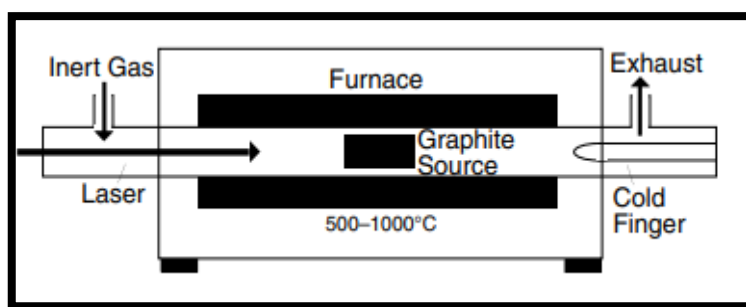
Figure 1.8 *Laser Ablation Method [19]*.

1.6.3.2 MWCNTs Synthesis by CCVD

Multi-walled Carbon nanotubes are most commonly synthesized through catalytic chemical vapor deposition (CCVD). Various research groups have been able to accurately manipulate the physical attributes of the carbon nanotubes produced through this process. Typically, nano-sized transition metal particles, including nickel, iron, cobalt, molybdenum, and copper, are used in CCVD as either oxide or metallic forms or as mixtures **(Figure 1.9)**. Their ability to catalytically decompose gaseous carbon-containing molecules is an essential property of these metal particles for carbon nanotube formation. Additionally, the size of the catalyst particles affects the solubility of carbon in them. The CCVD technique is affordable for producing carbon nanotubes at low temperatures, ranging from 300 to 1200 °C, and at normal atmospheric pressure. This versatile technique creates arrays of an individual or a mat of aligned carbon nanotubes, as well as a desired architecture of a nanotube device. Familiar gaseous carbon sources used are methane, acetylene, and carbon monoxide. For liquid carbon sources, alcohol like methanol and ethanol is heated in a flask and purged with an inert gas to carry the vapor into the reaction furnace. Alcohol-assisted growth has yielded single-walled carbon nanotubes at a relatively low minimum temperature of about 550 °C[24]**.**
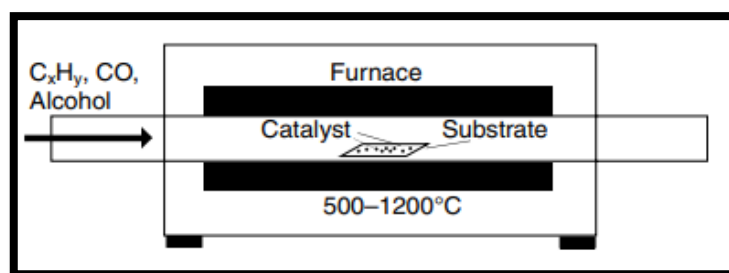
Figure 1.9 *Chemical Vapor Deposition [19].*

1.6.3.3 Purification of Carbon Nanotubes

CNTs prepared from arc discharge, laser ablation and CVD techniques contain various impurities such as amorphous carbon, fullerenes, graphite particles and metal catalysts. The presence of impurities can affect the performance of CNTs and their functional products significantly. Therefore, these impurities must be removed completely from nanotubes using appropriate methods[25]. Generally, the purification methods can be separated into physical methods and chemical methods. However, the separation method varies dramatically for nanotubes produced using different methods described above, since the type of impurities included in the raw samples are quite different depending on the production methods[19].

A. **Physical method:** Different morphology, aspect ratio, size, solubility, gravity, and magnetism of CNTs from those of impurities enable one to separate CNTs from impurities by using physical techniques such as filtration, chromatography, centrifugation, electrophoresis, and high temperature annealing[19].

B. **Chemical method:** Chemical purification of carbon nanotubes (CNTs) is a process used to remove impurities and contaminants from the CNT material, chemical purification of CNTs can include acid treatment, oxidative treatment, and sonication.

1.6.4 Structure of carbon nanotubes

CNTs are formed when graphene sheets (or hexagonal lattice) are coiled into seamless hollow cylinders[19]. In order to describe such a fundamental characteristic of the nanotube, two vectors **(Figure 1.10)**, Ch and T, whose rectangle defines the unit cell can be

23

introduced. Ch is the vector that defines the circumference on the surface of the tube connecting two equivalent carbon atoms, $Ch = n\hat{a}1 + m\hat{a}2$, where $\hat{a}_1$ and $\hat{a}_2$ are the two basis vectors of graphite and n and m are integers. n and m are also called indexes and determine the chiral angle which is used to separate carbon nanotubes into three classes differentiated by their electronic properties: armchair ($n = m, \theta = 30°$) with a C-C bonds parallel to the tube axis, zig-zag ($m = 0, n > 0, \theta = 0°$) with C-C bonds perpendicular to the tube axis, and chiral ($0 < |m| < n, 0 < \theta < 30°$) with a C-C bonds inclined to tube axis. Armchair carbon nanotubes are metallic (a degenerate semimetal with zero band gap). Zig-zag and chiral nanotubes can be semimetals with a finite band gap if ($n - m/3 = i$) (i being an integer and m $\neq$ n) or semiconductors in all other cases. The band gap for the semimetallic and semiconductor nanotubes scales approximately with the inverse of the tube diameter, giving each nanotube a unique electronic behaviour. Combining different diameters and chiralities results in several hundred individual nanotubes, each with its own distinct mechanical, electrical, piezoelectric, and optical properties[18].
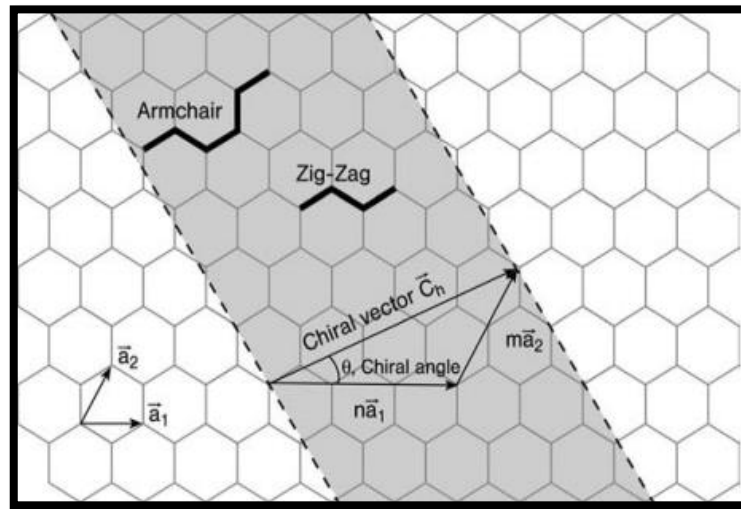
Figure 1.10 *Schematic diagram showing chiral vector and chiral angle in a rolled graphite sheet with a periodic hexagonal structure[25]*

1.6.5 Properties of carbon nanotubes

Carbon nanotubes are metallic or semiconducting depending on the diameter and chirality of the tubes, energy gap is inversely proportional to the diameter in semiconducting chiral CNTs. The band gaps of the CNTs vary from 0.2 to 1.2 eV. In SWCNTs conduction occurs through discrete electronic state, so it can be treated as quantum wires at extremely

low temperatures. CNTs are excellent conductors of electricity, with conductivity similar to that of copper. The electrical conductivity of CNTs is dependent on their diameter, chirality, and doping. Depending on their chirality and diameter, some CNTs can exhibit semiconducting properties. This means that they can be used in electronic devices such as transistors. CNTs have extremely low resistance due to their small size and lack of impurities. This property makes them useful in applications where low resistance is important, such as in interconnects and energy storage devices. CNTs can carry high current densities without heating up or melting, making them suitable for high performance electronic devices.

CNTs are among the strongest materials known, with a tensile strength up to 100 times greater than steel **(Figure 1.11)**. This high strength makes them ideal for applications where high durability and toughness are required. CNTs have an exceptionally high Young's modulus about 1 TPa , they are 6-7 times stiffer than steel, which means they are very resistant to deformation under load. CNTs are very lightweight, with a density about 1/6th that of steel. This low density makes them ideal for use in applications where weight reduction is important. They also have an excellent fatigue resistance, which means they can withstand repeated stress cycles without degradation.

Carbon nanotubes (CNTs) have several unique physical properties due to their nano-sized cylindrical shape and graphene-based structure. Some of the most important physical properties of CNTs include:

- **density** of SWCNT is 0.8 g/cm3 and it is 1.8 g/cm3 for MWCNT.
- **Length and diameter**: CNTs can vary in length from several nanometers to several millimeters, and in diameter from less than 1 nm to several tens of nanometers, depending on the method of synthesis.
- **High surface area:** CNTs have a very high surface area-to-volume ratio, which makes them ideal for use in applications such as catalysis, energy storage, and sensing.
- **High aspect ratio:** CNTs have an extremely high aspect ratio, which means that they are very long and thin. This aspect ratio contributes to their high strength and stiffness.
- **Optical properties:** CNTs exhibit unique optical properties, such as strong absorption and emission in the infrared region, which makes them useful in applications such as imaging and sensing.
- **Chemical stability:** CNTs are highly stable under a wide range of chemical conditions, making them useful in applications such as catalysis and drug delivery.

Property	CNTs
Physical Structure	Tube
Chemical Structure	Hexagonal
Interactions	π-π bond
Available Types	Single or Multiple walls
Dimensions	Single wall diameter = 1–2 nm
	Multi wall diameter = 4–20 nm
Elastic Modulus (TPa)	01 (axial direction)
Tensile Strength (GPa)	60–150
Thermal Conductivity (W/(mK))	3500
Electrical Conductivity (S/m)	3000–4000
Electrical Resistivity (Ω cm)	5×10^{-6} - 50×10^{-6}
Thermal Expansion (K^{-1})	Negligible in axial direction
Density (g/cm^3)	0.8
Electron mobility (cm^2/(V s))	$\sim 10^5$
Theoretical specific area (m^2/g)	1300
Thermal stability in air (°C)	700°C (in air); 2800°C (in vacuum)

Figure 1.11 *Properties of Carbon Nanotubes[26]*

1.6.6 Application of Carbon Nanotubes in the aeronautical industry

Materials used for the aeronautics applications are usually supposed to be strong, light, and thermal stable. As what is discussed before, CNTs contain almost all good properties that the aeronautics engineering is looking for[27]. The combination of structure, topology, and dimensions creates a host of physical properties in carbon nanotubes that are unparalleled by most known materials[21]. Here are some areas where CNTs can be utilized:

- **Conductive composites:** Metal and semiconductor CNTs have better electrical performance compared to traditional electronic materials. This makes them suitable for creating lightweight shielding for aircraft to protect against lightning and enhance technical electric systems.

- **Coating:** CNT coatings are being studied as a way to protect aircraft against the threat of ice formation, which can present a major security issue. These gripping coating surfaces can ward off adhesive ice problems, limit the utilization of substantial force required for removal during de-icing schemes and remove the extra bulk related with those solutions simultaneously. Moreover, the addition of CNTs in anticorrosion coatings for metals can enhance coating stiffness and strength[19].

- **Thermal conduction:** CNTs offer impressive heat conduction abilities and can be adopted within thermal interface materials, heat sinks, or composite parts for effectively modulating the thermal pressure of aircraft systems.

- **Structural material:** Carbon nanotubes show to be exceptionally useful for mechanical aims, surpassing the effectiveness of ordinary carbon fibers. Those fibers are already considerably tougher than steel, being applied for reinforcements in composite components including aircraft structures. Using nanocomposites' structural arrangement with nano-repeating distances between their parts, leading to weight reduction and fuel efficiency in aircraft. Carbon nanotubes prove advantageous due to the high surface area and aspect percentages in comparison to standard composites[17], [19].

1.7 Boron Carbide

Boron carbide has found suitability in multiple applications due to its advantageous combination of being both chemically stable with a low density while also coming with a high level of wearing properties and resistance against corrosion[28]. In the group of the most important non-metallic hard materials (alumina, silicon carbide, silicon nitride, diamond, or cubic boron nitride), boron carbide occupies a specific place[29].

1.7.1 Boron Carbide structure

The crystal structure of boron carbide (often B_4C) is rhombohedral **(Figure 1.12)**, consisting of 12-atom icosahedral located at the corners of the unit cell and the 3-atom linear chains that link the icosahedra along the (111) rhombohedral axis the composition of such a unit cell can be written as B6-C-C-C-B6 or B12C3[30]. The rhombohedral lattice parameters of B4C are a = 5.16 Å and $\alpha = 65.7$ Å, or, if represented as a hexagonal lattice, its lattice parameters become $a_0 = 5.60$ Å, $c_0 = 12.7$ Å with an axial ratio of $c0/a0 = 2.155$[31].
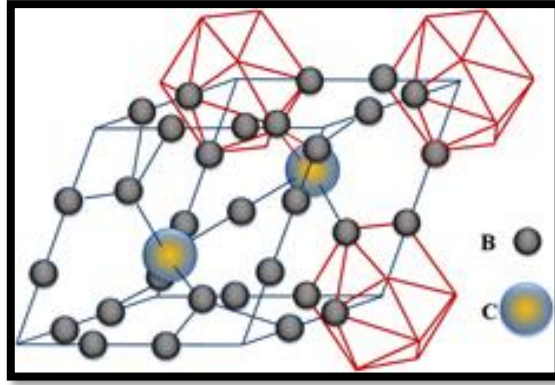
Figure 1.12 *Rhombohedral crystalline structure of boron carbide[32].*

The boron carbides consist of twelve-part icosahedral groupings that join with one another through both covalent bonds and inter icosahedral sequential alignments built up of three parts each. A single configuration exists for boron carbide materials which feature erratic carbon inclusion ratios[29]. The assemblage of the boron icosahedra and carbon atoms creates a perplexing configuration within the crystal matrix. This one-of-a-kind setup gives boron carbide unprecedented hardness, a high breakpoint, and excellent mechanical characterizations.

1.7.2 Properties of Boron Carbide

B4C is one of the lightest and the hardest material, making it a viable choice with respect to the reduced weight criterion in aerospace application. This table shows some of the important properties of Boron Carbide:

- **Chemical properties**: Boron carbide is one of the most stable compounds; its standard enthalpy of formations is low. Fine powders are slowly oxidized in wet air.
Boron carbide is not attacked by cold chemical reagents; it is oxidized by hot oxidizing acids (HNO_3, H_2SO, $HC104$, etc.) and fused salts[29].

- **Physical properties :** Boron Carbide has a low density which is in the range of 2.46 g/cm3 for B10.4C to 2.52 g/cm3 for B_4C and is determined by the light elements that form B_4C's crystal structure increasing linearly with increasing carbon content where slightly different stoichiometry is defined by either excess B or C.

The thermal expansion coefficient of B_4C is 5.73×10^{-6}/K in the temperature range of 300–1970 K[31]

Boron Carbide a p-type semiconductor through its entire homogeneity range.

- **Mechanical properties:** B_4C exhibits a strong anisotropy of the elastic constants, meaning that elastic moduli are orientation dependent. Typically, the Young's modulus values of dense B_4C ceramics, measured by acoustic techniques, are reported to be in the range of 460–470 GPa. however, a higher value of 570 GPa was also reported for 100% dense B_4C.

The Knoop hardness of B4C was reported to lie in the range of 28 GPa to 31 GPa .

The Vickers hardness was reported to vary in a broader range of 25 to 37 GPa, depending on the composition as well as the applied load used.

The fracture toughness, measured using the length of the cracks initiated from the corners of the Vickers impressions, is not very high and reported to be in the range between 2 to 3.5 MPa m1/2 depending on the grain size of B_4C.

In addition to measurements of fracture toughness using indentation techniques, the KIC of B4C has also been measured using the single edge v-notched beam, surface crack in flexure and chevron notch beam testing techniques, where similar values were obtained. The hardness of B_4C thin films measured by nanoindentation varied significantly in the range of 28 GPa to 60 GPa.

The indentation hardness of B_4C single crystals or polycrystalline ceramics was reported to be around 39–55 GPa as measured using a Berkovich indenter.

The flexural strength of B_4C is not very high and is reported to be around 250–450 MPa, while compressive strength is much higher and lies in the range of 6.1 ± 0.3 GPa[31].

1.7.3 Main Application of Boron Carbide in Aerospace

Heat and radiation shielding: Boron carbide is an important type of neutron radiation shielding material with relatively high efficiency due to the high content of B element[33] which has an ability to absorb and attenuate radiation for ensuring the safety of astronauts and sensitive equipment.in addition, Boron carbide ceramic materials have impressive characteristics that include being able to bear a high temperature of up to 1970°C, showing a low coefficient of thermal expansion which makes them suitable for exploitation
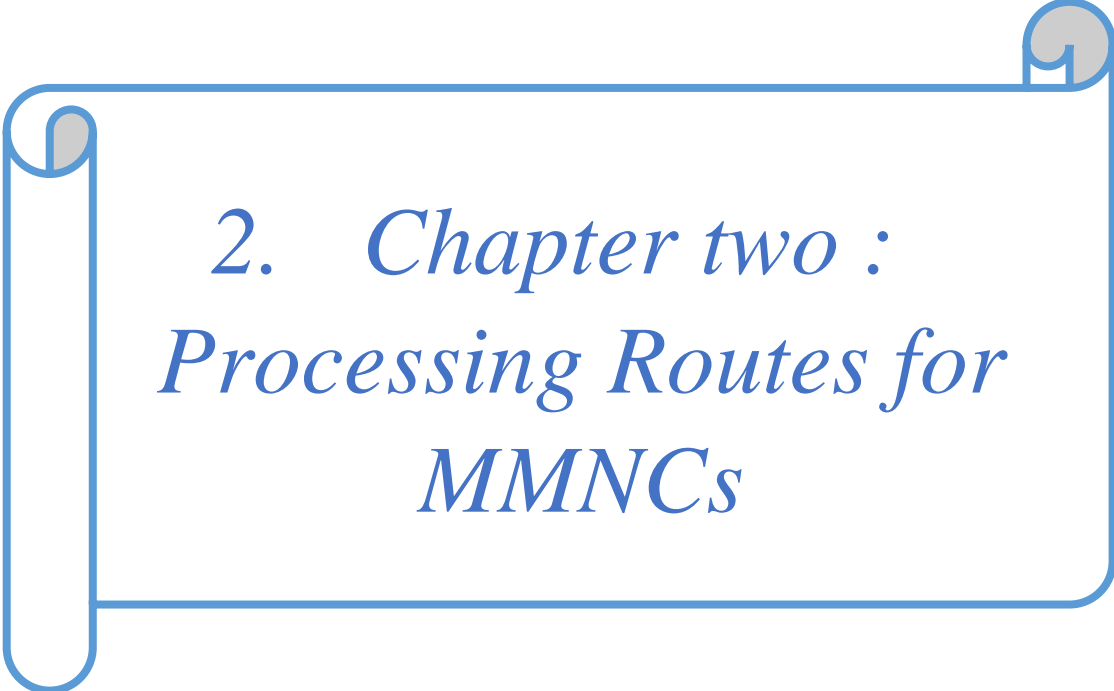
as heatsinks, and withstanding various conditions so well over extended periods that they can be recycled indefinitely without causing environmental damage[34].

Armor systems: Boron carbide is commonly used in ballistic armor for aircraft and spacecraft because of its tough resistance and lightweight, effectively protecting against powerful impacts .B_4C is probably the best overall ceramic material, particularly in areal density, it also has the highest modulus of elasticity which -it has been hypothesised- is related to its ability to spread the bullet's energy over a greater aera. However, B_4C's higher cost production makes it very cost-sensitive[35].

Structural components: Boron carbide is a highly suitable material for aerospace applications due to its exceptional strength-to-weight ratio and resistance to corrosion and wear. It is commonly used for constructing lightweight and durable brackets, bushings, and nozzles. Additionally, incorporating boron carbide-reinforced components enhances aerospace equipment's structural integrity and energy efficiency.

The aerospace industry utilizes boron carbide in several ways due to its exceptional properties, which make it an essential material for different critical applications. These are only a few examples of its applications.

2. Chapter two : Processing Routes for MMNCs

The main difficulty in working with nanocomposites lies in their production and processing. Ideas for dispersing the tiny reinforcements within the matrix and securely bonding them together are challenged. Many processes of creating these composites need to adequately paint both requirements, leading to clusters of unbound reinforcement, reducing how well it functions when exposed to environments like high temperature and pressure.

Processing nanocomposites can be challenging and may result in various issues that require attention to achieve high-quality materials with desired properties. Common problems that may arise during the processing of nanocomposites include:

- Uneven dispersion and agglomeration
- Brownian motion
- Inter-particle forces, Van-der Waals, and electrostatic repulsion
- Interface debonding
- Brittling of the composites due to the filamentous shape of the reinforcements
- Porosity and distortion in the final component
- Wear action of the reinforcements on the cutting tools
- Contamination causing by refractory effects of metals as aluminum
- Occurrence of chemical reaction as a consequence of converting mechanical energy into thermal energy

2.1 Strengthening Mechanisms

The yield strength (YS) of metallic materials is determined by the stress required to move dislocations and activate dislocation sources. This strength is affected by the obstacles that restrict dislocation motion. Different approaches have been proposed to predict the bulk mechanical properties of MMNCs based on the reinforcement, matrix, and processing routes[9]. These approaches consider strengthening mechanisms that enhance the mechanical properties and strength of the composite material. These mechanisms are crucial in improving the overall performance and functionality of nanocomposites. They consider one or more of the following strengthening mechanisms:

- *The Orowan strengthening mechanism:* relies on applying stress to overcome obstacles, such as particles, to force dislocations to bypass them. This stress is caused

by the resistance of closely spaced hard particles that dislocations encounter as they pass through. When the particles are coarse, and the inter-particle spacing is large, the Orowan effect is minimal. However, highly dispersed nano-sized particles make Orowan strengthening more effective, resulting in improved creep resistance and thermal stability[36].

- *The Enhanced Dislocation Density:* the matrix and reinforcement materials have different coefficients of thermal expansion; thermal stresses occur around the particles during the cooling process. This can lead to plastic deformation, particularly in the interface region between the matrix and reinforcement. This phenomenon is known as enhanced dislocation density[9].

- *The load bearing effect:* refers to the transfer of load from the soft matrix to the rigid ceramic particles. A strong cohesion between the matrix and reinforcement is necessary for this reinforcing mechanism to be effective[9].

- *The Hall-Petch effect:* is a widely recognized mechanism that strengthens materials by decreasing grain size.

$$\sigma_y = \sigma_0 + kd^{-1/2} \quad \ldots\ldots(2.1)$$

Equation (1) shows that as grain size (d) decreases, the material's strength σ_y increases, with σ_0 representing the original strength (in MPa) and k a constant (in MPa $\sqrt{}$ m) that varies depending on the material. In nanocomposite materials, the matrix's grain size depends on the nanoparticles' particle size and volume fraction. The matrix's grain size reduces as the particle size decreases or the volume fraction increases. Adding a large amount of Y_2O_3 reinforcement to the matrix increases grain boundary pinning, resulting in grain refinement. The Zener equation (2) expresses the relationship between the matrix's grain size, particle size d_p, and particle volume V_p, with ، where α is a proportionality constant. However, the equation is not applicable when the particle volume or size approaches zero and has some limitations[37].

$$d_m = \frac{4\alpha dp}{3Vp} \quad \ldots\ldots(2.2)$$

Considering all these factors, we can estimate how the mechanical properties increase when the size decreases.

2.2 Modelling Yield Strength (YS)

There are a lot of modelling methods to predict the yield strength of particle-reinforced Metal Matrix Nanocomposites[38]. Three main models have been proposed: *Arithmetic Summation, Quadratic Summation*, and *Compounding Methods*. Summation methods use dislocation theory to account for obstacles to dislocation motion on the same structural scale and at significantly different scales, with quadratic and arithmetic summation being adopted for each, respectively. Based on the modified shear lag mechanism, the compounding method treats all strengthening mechanisms as load-transferring mechanisms from the matrix to the reinforcement and is represented mathematically by a series of improvement factors (fi)[9].

Some experts have suggested an *Arithmetic Summation*, a straightforward mathematics scheme for estimating the yielding strength of aluminum composite materials containing assorted particles. This technique presumes every factor influences their effect individually. Thus, adding them all up results in the potential final value of strength for such composites through the formula included here[38]:

$$\sigma_{yc} = \sigma_{ym}(1 + f_l)(1 + f_d)(1 + f_{orowan})\ldots\ldots(2.3)$$

Where σ_{yc} is the yield strength of the MMCs, σ_{ym} is the yield strength of the unreinforced matrix, f_l is the improvement factor related to load-bearing effect, f_d is the improvement factor related to the dislocation density in the matrix, and f_{orowan} improvement factor related to the Orowan strengthening[9].

Quadrature summation consists of the sum of squares of the different mechanisms contribution, the improvement of yield strength with this method can be expressed as follows[9]:

$$\Delta\sigma = \sqrt{(\Delta\sigma_{load})^2 + (\Delta\sigma_{CTE})^2 + (\Delta\sigma_{EM})^2 + (\Delta\sigma_{Orowan})^2 + (\Delta\sigma_{Hall-Petch})^2} \ldots\ldots(2.4)$$

Where , the incremental contribution to YS by the load bearing effect can be expressed as:

$$\Delta\sigma_{load} = 0.5\, V_p\, \sigma_{ym} \dots\dots(2.5)$$

The effect of mismatch strain due to the difference between the CTE values of particles and that of the matrix is given by the Taylor expressing the increase in geometrically necessary dislocations as detailed in:

$$\Delta\sigma_{CTE} = \sqrt{3}\beta G_m b \sqrt{\frac{12 V_p \Delta\alpha\Delta T}{b d_p}} \dots\dots(2.6)$$

The strength improvement by the modulus mismatch is approximated by:

$$\Delta\sigma_{EM} = \sqrt{3}\alpha G_m b \sqrt{\rho E_m} \dots\dots(2.7)$$

Avec :

$$\rho E_m = \frac{6 V_p}{b d_p \varepsilon} \dots\dots(2.8)$$

The increase in the material yield stress due to the Orowan mechanism can be expressed as:

$$\Delta\sigma_{Orowan} = \frac{0.13 G_m b}{\lambda}\, ln\frac{dp}{2b} \dots\dots(2.9)$$

Avec :

$$\lambda = d_p \left[\left(\frac{1}{2V_p}\right)^{\frac{1}{3}} - 1 \right] \dots\dots(2.10)$$

The incremental contribution of grain refinement to the strength levels can be estimated on the basis of the classical Hall-Petch equation:

$$\Delta\sigma_{Hall-Petch} = k d_m^{-1/2} \dots\dots(2.11)$$

With :
- V_p : volume fraction of Particle Reinforcements
- σ_{ym} : Matrix yield strength

- β : strengthening coefficient is considered to be 1.25
- G_m : shear modulus
- b   : the Burgers vector
- $\Delta\alpha$: the difference between CTE of matrix and particles
- ΔT : the difference between the processing and the tensile test temperatures
- α : the material-specific coefficient
- ε : the bulk strain of the composite
- k   : Hall-Petch coefficient
- d_m : the matrix grain diameter
- d_p : diameter of the reinforcement particles
- λ : the inter-particle spacing

2.3 Production Routes for Metal Matrix Nanocomposites

Two main methods are involved in creating Metal Matrix Nanocomposite: ex-situ and in-situ. In-situ involves infusing elements during fabrication, while Ex-situ involves adding reinforcements externally. The following few paragraphs will provide a basic overview of the in-situ procedure. We will then further flesh out the essential ex-situ processing techniques with a specific focus on Mechanical Alloying, the ideal manipulation process for our combination of reinforced aluminum-based Metal Matrix along with CNTs and B4C.

2.3.1 In-situ approaches

In-situ manufacturing methods offer several advantages, such as high thermodynamic stability at high temperatures, which leads to a clean interface between the particle and matrix and robust interfacial bonding. It also eliminates harmful phases and facilitates nascent interface creation through process control, enhancing wear resistance; additionally, smaller particle sizes in the nanocomposite result in superior mechanical properties due to improved distribution. Furthermore, the process can produce composites with matrix materials (aluminum, titanium, copper, nickel, and iron) and reinforcing particles (borides, carbides, nitrides, oxides, and their mixtures), making it cost-effective and scalable. However, commercial applications have been restricted due to the complexity of

reactions and the need for more knowledge concerning these techniques. Reactive and morphological processes are the two categories of In-Situ approach:

Reactive processes in solid-liquid state: Elements or compounds react in a third liquid metallic phase that acts as a solvent medium. The diffusion of components in the metal matrix generates the reinforcement.

Reactive processes in the liquid-liquid state: The MixAlloy Process produces nanocomposite materials by combining two streams of metal melts containing ceramic inclusions in a reaction chamber to form refractory particles. These particles are then rapidly cast or atomized.

Reactive processes in the gas-liquid state: The gas-liquid process involves injecting gas into a melt metal with one or more elements to create a reinforcement phase chemically. Refractory elements can also be added for custom precipitation[9].

Morphological processes: The term "morphological process in-situ" refers to the way in which nanocomposites are created within a matrix. This method allows for precise control over the morphology of the nanocomposite during its formation. It involves using chemical reactions or physical processes to control the growth and distribution of nanoparticles within the matrix. For instance, metal matrix nanocomposites can be created through selective laser melting (SLM), where particles are reinforced into the metal matrix; the process involves using a laser to melt and solidify layers of metal powder containing nanoparticles carefully. This results in precise control over the distribution and shape of the nanoparticles within the metal matrix. Another example of this method is using chemical methods, such as the sol-gel process, to create metal matrix nanocomposites with controlled microstructure and morphology[39], [40].

2.3.2   Ex-situ approaches

2.3.2.1   Liquid state Routes

1) Stir casting

Stir casting is a process used to produce metal matrix composites by mixing reinforcement material with a matrix material. This process is cost-effective, suitable for mass production, and allows easier control of the composite structure. The stir-casting setup typically includes a furnace for heating and melting the materials, a reinforcement feeder, and a mechanical stirrer. The stirrer forms a vortex to mix the reinforcement material with the melt and is typically controlled by a variable-speed motor. The feeder is used to introduce the reinforcement powder into the melt. Different types of molds can be used for pouring the mixed slurry, including permanent, sand, or lost wax molds.

The stir casting process is almost net shaping, meaning it requires little post-processing, and it is a popular choice for producing metal matrix composites. The stir-casting process involves several steps, as shown in **(Figure 2.1).** First, the matrix material is melted in a bottom pouring furnace, while the reinforcements are preheated in a separate furnace to remove any impurities or moisture. Next, mechanical stirring is initiated to create a vortex once the matrix material has melted at a specific temperature. The reinforcements are then poured into the vortex at a constant feed rate using a feeder, and the stirring process continues for a set period after the reinforcements have been fully added.

The molten mixture is poured into a preheated mold and left to cool and solidify naturally. Post-casting processes such as heat treatment, machining, testing, and inspection may also be performed. Impeller blade geometries can vary for this process, and melting the matrix material is the first step[41].
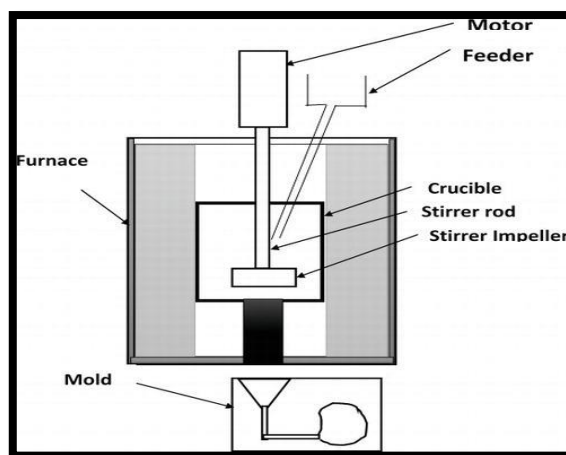
Figure 2.1 Typical stir casting experimental set-up[41]

2) Ultra sonic assisted casting

Ultra sonic assisted casting **(Figure 2.2)** is reported to be effective in eliminating particle clusters generated due to agglomeration tendency and low wettability of nanoparticles[42]. Sonochemistry permits the production of novel materials or provides a route to known materials without needing high bulk temperatures, pressures, or long reaction times. Both chemical and physical phenomena associated with high-intensity ultrasound produce or modify nanomaterials[43]by treating the melt with ultrasonic waves (usually in the frequency range of 18–20 kHz) during or after adding the reinforcing phase. High-intensity ultrasound provides a unique interaction between energy and matter[44].
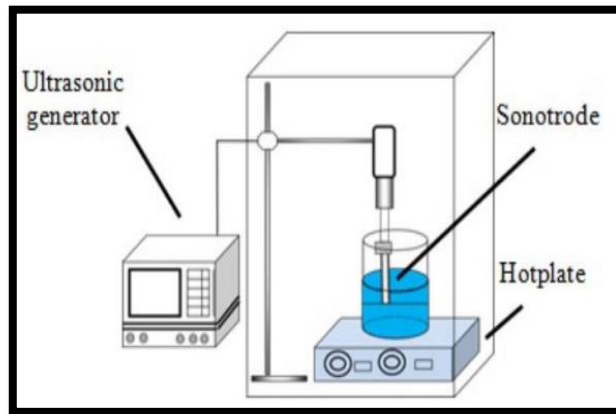

Figure 2.2 Ultrasonic assisted casting set-up

3) High pressure die casting

High Pressure Die Casting (HPDC) **(Figure 2.3)** is a near-net shape manufacturing process in which the molten die-cast metal is injected into a metal die cavity at high speed, solidified under high pressure, and has a high cooling rate of 500–1000 K/s. HPDC has been widely used in producing lightweight die-cast aluminum and magnesium alloy components with high dimensional accuracy, high production efficiency, and low cost for automotive, aerospace, and other industries. However, the turbulent flow under high-speed injection and the consequent entrapment of air during die filling are inherent problems for the currently used conventional non-vacuum assisted HPDC process, which results in the formation of gas porosities in HPD castings. The gas porosities will expand and blister when exposed to high temperatures, making conventional HPDC castings unavailable for further

strengthening through high-temperature heat treatment. Therefore, most HPDC castings must be used in an as-cast state[9].
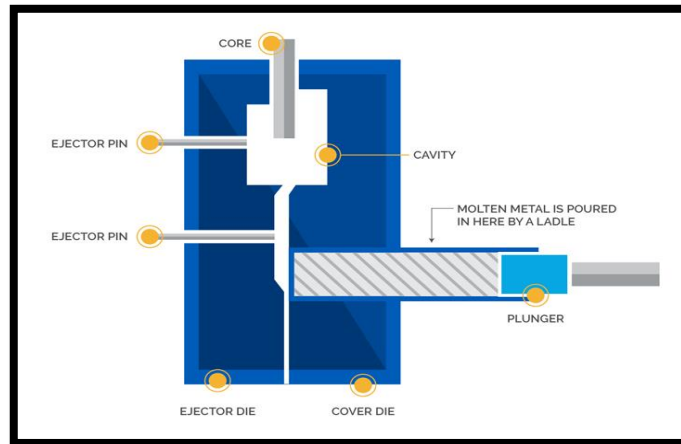
Figure 2.3 *Schematic of the HPDC process[45]*

4) Disintegrated melt deposition:

The Disintegrated Melt Deposition (DMD) **(Figure 2.4)** method is used to create metal matrix nanocomposites. The metal matrix and nanoparticles are heated in a crystallizing growler within an inert gas environment. Next, a pressurized gas stream breaks down the melted combination into tiny droplets. These droplets are then deposited onto a holder material, resulting in a potentially significant composite material. DMD combines spraying techniques and innovative fusion to produce metal matrix nanocomposites with consistent microstructures and shapes[46].
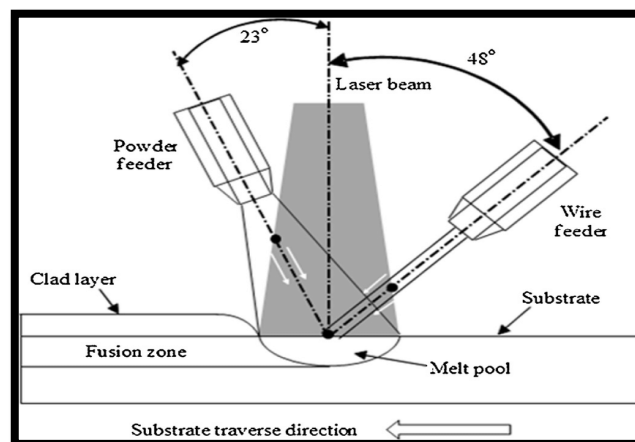
Figure 2.4 *Schematic of the DMD process with simultaneous wire and powder feed[47]*

2.3.2.2 Solid state Routes

1) Powder Metallurgy

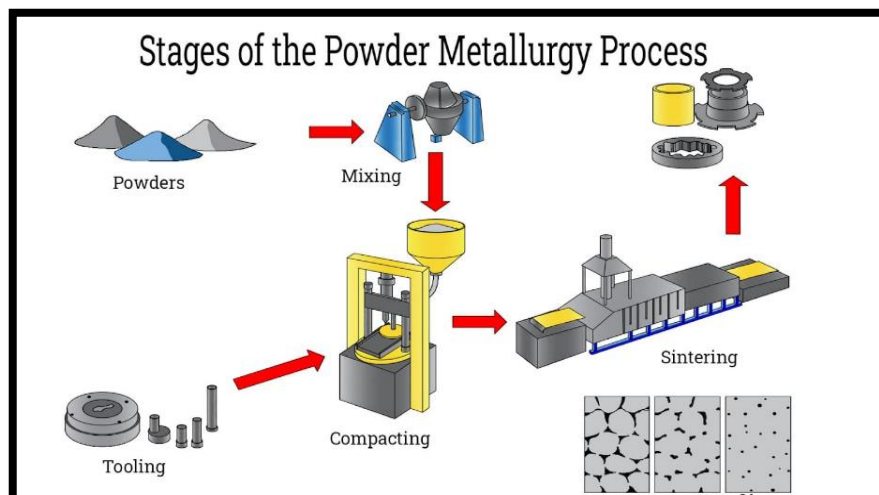Powder Metallurgy (PM) **(Figure 2.5)** processes, usually involve the following phases: blending of matrix alloy and reinforcing phase powders; compacting the blend, usually by cold pressing; degassing the compacted structure to remove volatile contaminants (lubricants, mixing and blending additives), water vapor and gases; green compacts can be then consolidated by different routes such as direct sintering, hot isostatic pressing (HIP), vacuum hot isostatic pressing, hot extrusion or cold sintering[9]. The advantages of the process are flexibility and the ability to produce near-net shaped components. The size range of metal powders available on the market is quite wide which it is an advantage[36]. Some issues that occur during the processing is the increasing of the agglomeration although it can be minimized only if the size of the matrix powder is in the size range of the reinforcement phase. In addition, further working of the product via P/M may cause the reinforcement phase to break up and deform the surrounding matrix, leading to stress concentration and cracking[36]. In order to obtain high density parts, it is better to increase the sintering temperature, which sometimes can be even higher than 90% of the melting temperature. The welding together of the particles occurs by atomic diffusion and generates the strength required for application.

Figure 2.5 *Powder Metallurgy Process[48]*

2) Mechanical alloying

a) History and principle of Mechanical Alloying

The mechanical alloying process was invented at INCO's Paul D. Merica Research Laboratory around 1966. The initial attempt was to develop a material by combining oxide dispersion strengthening with gamma prime precipitation hardening in a nickel based superalloy for gas turbine applications and other heat resistant alloys. As the oxides could not be dispersed in the liquid phase, a solid state processing technique was therefore needed. In the early 1960s, INCO's Pual D. Merica Research Laboratory had successfully coated nickel onto graphite surface using this technique. The coated graphite particulates were injected into molten aluminum alloys using an argon sparging gas. At this stage, this process was referred to as "milling/mixing". The term "mechanical alloying" was later introduced by E. C. MacQueen in the late 1960's[49].

In the last ten years, the method of high-energy milling gained much attention as a non-equilibrium process able to produce nano-scale microstructures. Various mills have been developed for different purposes, including tumbler, attrition, shaker, vibratory, and planetary mills[36]. In the traditional PM process, the blending aims to mix the powders without inducing material transfer between the mixed components. However, It is possible to perform high-energy mixing through milling media to eliminate the voids between the matrix and the reinforcement powders by incorporating hard ceramic particles into the matrix powder through a solid-state bonding. For example, in mechanical alloying (MA), matrix and reinforcement are fused by inducing cold welding, fracturing, and re-welding of the powder particles[9]. Making metallic alloys stronger involves reducing the grain size and propagating nanosized particles. For this process, a small part of the base powders is mixed with grinding media in an airtight container. Then, they are amalgamated through vigorous shaking for a measured period. The amount of energy the grinding balls have is determined by their mass and speed, so it is best to use dense materials like stainless steel and tungsten for a higher yield. The elements of the process which influence the outcome the most are how many balls there are relative to the powder ratio, how long it runs, and how fast the milling cylinder rotates. Once the materials are ground into powder, they are compressed without other gases and solidified once more.

b) Types of Mills techniques

Mechanical alloying stands out as a one-of-a-kind approach that can be executed under ambient conditions, whether high or low-energy alternatives. Different types of milling equipment are available for particle size reduction, mixing or blending, particle shape changes, and production. They differ in capacity, milling efficiency, and additional arrangements for heat transfer[50].

SPEX Shaker Mills: Shaker mills such as SPEX mills **(Figure 2.6)**, which mill about 10-20 g of the powder at a time, are most commonly used for laboratory investigations and for alloy screening purposes. These mills are manufactured by SPEX CertPrep, Metuchen, NJ. The common variety of the mill has one vial, containing the sample and grinding balls, secured in the clamp, and swung energetically back and forth several thousand times a minute. The back-and-forth shaking motion is combined with lateral movements of the ends of the vial. With each swing of the vial the balls impact against the sample and the end of the vial, both milling and mixing the sample. Because of the amplitude (about 5 cm) and speed (about 1200 rpm) of the clamp motion, the ball velocities are high (on the order of 5 m/s) and consequently, the force of the ball's impact is unusually great. Therefore, these mills can be considered as high-energy variety[51].
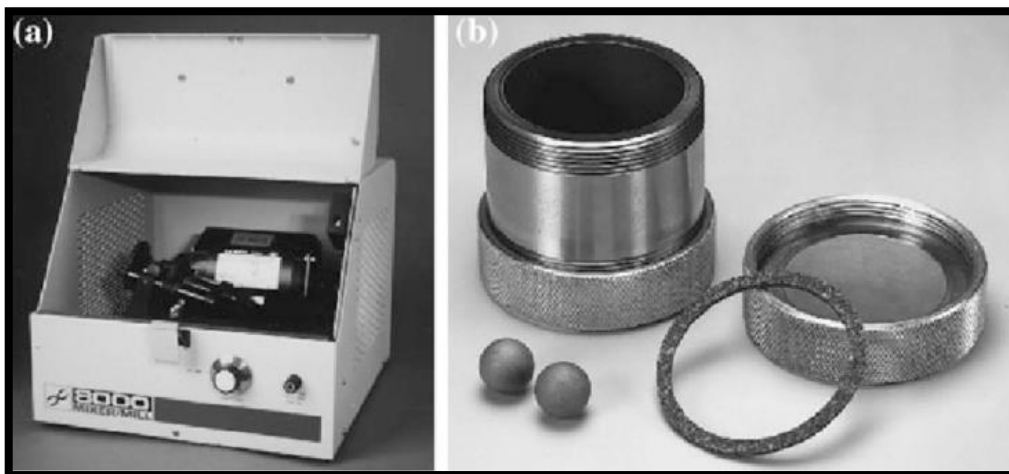
Figure 2.6 (a) SPEX 8000 mixer/mill in the assembled condition. (b) A vial and balls[52]

JET Mills: Jet milling **(Figure 2.7)** is a common mechanical practice without the need for solvents and able to be done on a large scale that can be done with either wet or dry materials.

Traditional dry jet milling is generally applied to reduce the size of dry substances, resulting in fine powders up to 10 microns in size. The process breaks down matter using particles crashing into one another through continuous attrition, absence of heat, or damage from wearing away; this favors the fragmentation of aggregates. Jet milling was more productive than extrusion in creating nanocomposites with enhanced thermal and mechanical characteristics, which was predictably linked to the extent of nanoparticle dispersal. Using jet-milling, the distribution of nanoparticles was functioning effectively no matter what number of fillers were utilized, decreasing the average size of fillers, and exhibiting improved saturation with alumina. Subsequent mechanized assessment and fracture examination told of improvements within yield rating and variances in elasticity, reiterating how the steady nanofoam rewarded promising results. This suggests jet milling is more efficient and research-based than extrusion for preparing nanocomposites with polymers. This finding is based on a reduction in ductility which, with increasing levels of alumina, was observed only in samples produced by extrude but not those created by jet milling despite the fragility that most nanofilaments contribute to. This difference can be accounted for due to the entire decline of damage surrounding caplets milled with[53].

Figure 2.7 Micronization Mill/ Spiral Jet Mill[54]

Cryogenic Mills: Cryomilling **(Figure 2.8)** is a process in which milling is done at shallow temperatures, often with a cryogenic medium like liquid nitrogen. A PCA (such as stearic

acid) can be used to prevent sticking. During traditional milling, the friction causes the temperature to increase, leading to the recovery and recrystallization of fine microstructures. However, cryomilling suppresses these effects due to its low temperature, resulting in finer grain structures and more rapid grain refinement. This can lead to nanocrystalline grain structures. In addition, harmful chemical reactions between the matrix and reinforcement are also suppressed at these low temperatures. See **(Figure 2.8)** for a schematic of the cryomilling process[9].


Figure 2.8 Cryogenic Mill - Cryomill[55]

Tumbler Mills: A conventional tumbler ball mill **(Figure 2.9)** consists of a rotating horizontal vessel partially filled with steel balls. The vessel, whose length exceeds its diameter, is fitted with shafts, and rotated about its longitudinal axis. As the vessel rotates, the balls drop on the powder that is being ground. By increasing the diameter of the mill, the efficiency of operation increases. This is caused by the greater height of the fall and the impact energy imparted to the grinding media. The rate of grinding increases with the speed of rotation. At high speeds, however, the centrifugal force acting on the steel balls exceeds the force of gravity, and the balls are pinned to the wall of the vessel[50].
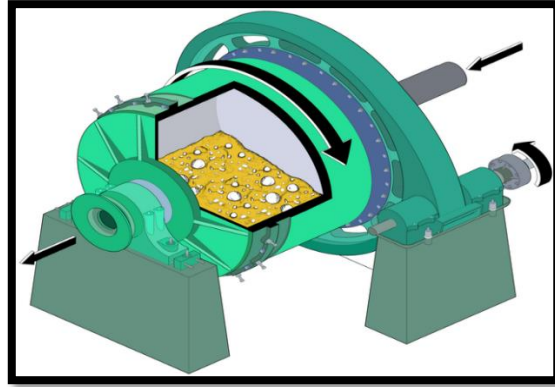
Figure 2.9 Tumbler Mill[56]

Attritor Mills: A conventional attritor mill **(Figure 2.10)** consists of a rotating horizontal drum half-filled with small steel balls. As the drum rotates the balls drop on the metal powder that is being ground, the rate of grinding increases with the speed of rotation. At high speeds, however, the centrifugal force acting on the steel balls exceeds the force of gravity, and the balls are pinned to the wall of the drum. At this point the grinding action stops. An attritor (a ball mill capable of generating higher energies) consists of a vertical drum with a series of impellers inside it. Set progressively at right angles to each other, the impellers energize the ball charge, causing powder size reduction because of impact between balls, between balls and container wall, and between balls, agitator shaft, and impellers. Some size reduction appears to take place by interparticle collisions and by ball sliding. A powerful motor rotates the impellers, which in turn agitate the steel balls in the drum[51].
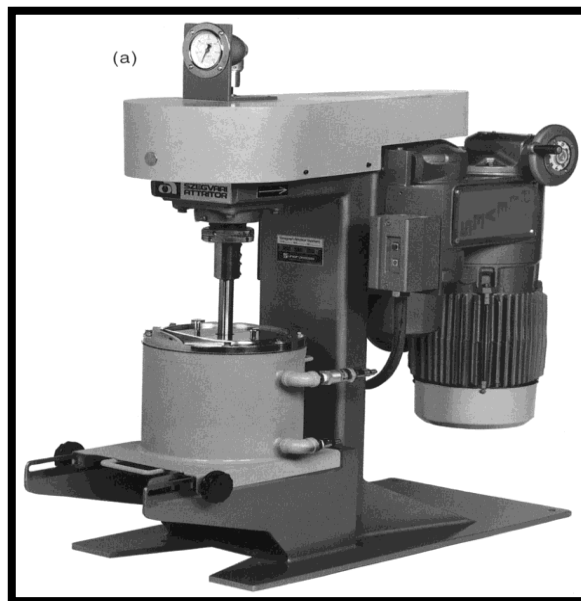
Figure 2.10 Attritor Mill[57]

46

Planetary Ball Mills: Another popular mill for conducting MA experiments is the planetary ball mill in which a few hundred grams of the powder can be milled at a time[51]. The planetary ball mill owes its name to the typical orbital revolution movement of its vials. These are arranged on a rotating support disk, and a special drive mechanism causes them to rotate around their own axes. To create fine metallic nanocomposite powder, metallic and reinforcing particles (nanomaterials) are mixed and ground in a sample jar with a large number of balls. Repeated collisions between the particles, balls, and vessel walls break down the material into nano-powder through compression, shear, and frictional forces. This process prevents agglomeration and ensures a homogeneous distribution of compounded particles into the matrix **(Figure 2.11)**. During milling, the compounding particulates become finer while the matrix phase is deformed plastically. The metal may become flattened and welded together, while the fragmented reinforcing material is embedded between metallic particles. The properties of the ball-milled nanocomposites depend on matrix strength, nanofiller dispersion, porosity, active surface area, interfacial interactions, and reactions. Efficient interfacial bonding can be achieved by modifying the wettability angle at the interface, typically done through the sintering process[58].
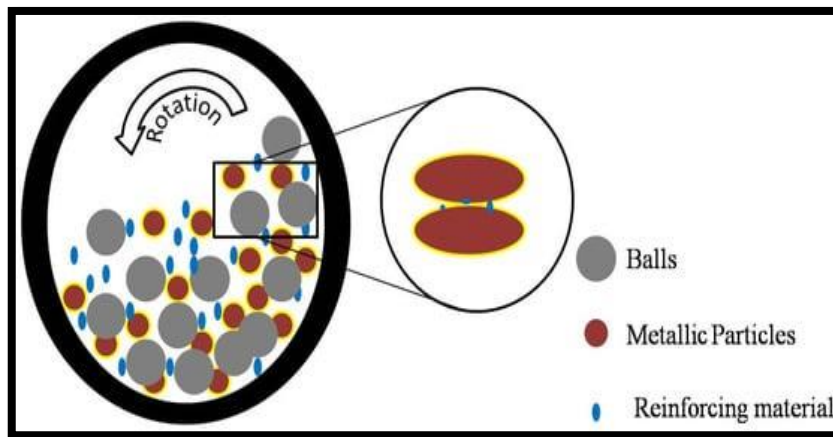
Figure 2.11 *Schematic of metallic nanocomposite ball milling process. Inserted: the particle embedded onto the interfacial boundaries of the metallic matrix after mechanical alloying[58].*

c) The Main Steps in Mechanical Alloying Process

Nonequilibrium processing of materials starts with energizing the material and using that excited (high-energy) state to process the materials to obtain the desired microstructure and properties. Researchers have traditionally used temperature, pressure, light, or electricity to transform the equilibrium material into an energized condition. However, an easy and

unconventional method to energize a material is to use "brute force" (or mechanical stress). The so-called severe plastic deformation processes (note that this name and the different variants under this category have come around much later than the mechanical alloying technique) subject the material to high impact, shear, and torsional forces to energize the material.

During the process of MA, it is crucial to combine individual elemental powders or pre-alloyed powders with a grinding medium in a high-energy ball mill. A ball-to-powder weight ratio of 10:1 or higher must be maintained to ensure the desired outcome. This process involves repeated cold welding, fracturing, and rewelding of powder particles. Balancing the fracturing and welding events makes it possible to control the resulting powder size. When fabricating ductile metals, using about 1-2 wt.% of a process control agent (PCA) is imperative. The PCA adsorbs on the surfaces of the powder particles to minimize excessive cold welding among themselves and to the milling container and the grinding medium, which inhibits the agglomeration of powder particles. As the milling time progresses, the particle and grain sizes decrease gradually, eventually reaching nanometre levels[59]. A precise amount of the result powder is pressed into a die to create the desired shape. This pressure can be applied in either cold or hot conditions. The resulting compact will have some porosity, which can be reduced through various methods. Sintering is a standard method that involves heating the compact at temperatures below the material's melting point. During this process, surface and grain boundary diffusion, evaporation, and condensation occur, resulting in densification and the elimination of pores[18].

The process of MA can be carried out in small capacity and high-energy mills (SPEX mills) to produce about 10–20 g per run for alloy screening purposes, in medium-energy planetary mills to produce about 200–500 g at a time, or in low-energy much larger mills (attritors) to produce kg quantities. High-energy and high-speed mills that can produce about 5,000 kg of powder per hour are also available[59].

d) Factors Affecting the Properties of Mechanically Alloyed Nanocomposites

➢ **Time duration of milling** is a vital parameter in the ball milling process in the phase formation, microstructural distribution, and homogenous distribution of components or ingredients. It also influences the physicochemical-mechanical properties of the

composites. The size of the nanomaterial (reinforcing material) reduces with an increase in milling time[58].

➢ **The rate of milling** has a great effect on the measurements of particles and grain boundary size. By increasing the milling speed, the size of particles lessens by consequence. At a reduced rotary speed, the adhesion at the interface of Copper with CNT nanoparticles was found to be feeble. An increased rotary velocity was linked to a downscaling of the particle's crystalline size. Results at lower cutting velocities had few blemishes and unevenness, whereas faster milling induced strain hardening and decreased the hardening due to heat.

➢ **A higher amount of energy** is indeed needed during milling for efficient incorporation of nanofillers into the matrix. When dry milling is utilized, the crystals are typically of a smaller size. However, the use of a solvent can counters the effects of energy limitation when wet production processes are involved.

➢ **The ball-to-powder ratio** is an important and fundamental parameter of milling operations. Smaller diameter balls (measuring 10mm or smaller) result in higher efficiency when milling, as the number of times the balls and grinding media interact increases. As such, more shearing forces are created and this subsequently has a great effect on the size of crystals, the amount that can be produced, as well as how much energy is expended. This increases with an increase in time. In contrast to this, when the size increases, the weight of the ball also increases, which infuses greater kinetic energy. The kinetic energy has a direct impact on the ball size. As the size of the balls increases, the amount of free space also increases exponentially; this could be resolved with a mixed ball size combination[60].

➢ **The higher concentration of reinforcing material** leads to higher deformation and micro hardening of the matrix phase. This accelerates the fracturing and welding processes and promotes the process of milling to be completed in a briefer duration since the grain growth of metal is inhibited by the nanoparticles[58]

e) The Gloves Box

The glove box **(Figure 2.12)** is designed to handle oxygen-sensitive products. It operates in a closed circuit with an inert argon atmosphere isolated from the outside environment. An airlock prevents contact with the outside atmosphere by retracting the material with a vacuum pump. The airlock has two doors - one connecting to the glove box and the other to the outside. To use it, we first ensure that the inside door of the airlock is properly closed. Then we insert the material onto the sliding tray and close the outside door. After creating a vacuum, we fill the airlock with argon and open the inside door to insert the material.

Figure 2.12 *The Gloves Box [61]*

2.4 Elaboration of the Al-2w%MWCNTs-2w%B$_4$C by mechanical alloying

Aluminum matrix reinforced with the same weight percentage of both MWCNTs and B$_4$C at different processing time were successfully processed by mechanical alloying.

A Planetary Micro Mill Pulverisette 7 **(Figure 2.13),** was used for the milling of the Al-2w%MWCNTs-2w%B$_4$C nanocomposites at different processing times of 15, 30, and 60 minutes.

Figure 2.13 Planetary Micro Mill Pulverisette 7[62]

Samples of 3g of elementary powders (0.06)g of MWCNTs, (0.06)g of B_4C and (2.88g) of commercial Al powders (99.95% purity),were milled at a speed milling of 350 rpm with a ball to powder ratio of 10:1. The milling was carried for different milling time of 15, 30 and 60 minutes in presence of 2% of process control agent (PCA). The methanol which was used as PCA was added to avoid excessive cold welding of aluminium powders during milling process. After 5 minutes of running the ball mill was given an interim period of 5 minutes to avoid overheating. The effect of milling time on powder morphology and the particle size was studied by taking small amount of hybrid nanocomposite from each sample.
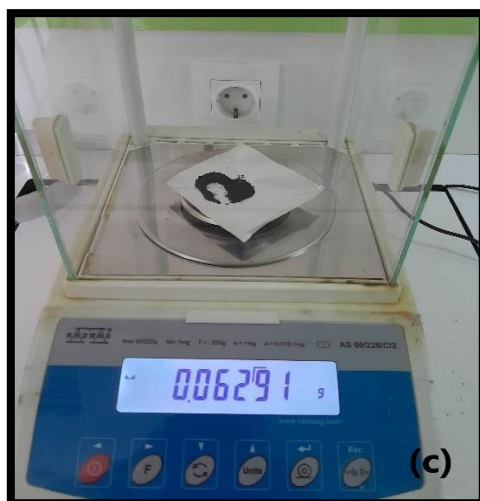
Figure 2.14 weighing of elementary powder (a) aluminum, (b) MWCNTs and (c) B$_4$C.

The powders produced during the process can be contaminated at various stages of milling. This can be due to factors such as the level of cleanliness of the equipment used, the impact of collisions between bills and jars resulting in material spalls, and the effect of the atmosphere and chemical reactions. To minimize contamination during the milling process the masses of the elemental powders are slightly exceeded to obtain a final mass of the composite close to the initial mass envisaged.

After repeated collisions between the particles, balls, and vessel walls break down the material into nano-powder through compression, shear, and frictional forces, the specimens were then consolidated by high cold pressure **(Figure 2.15).**
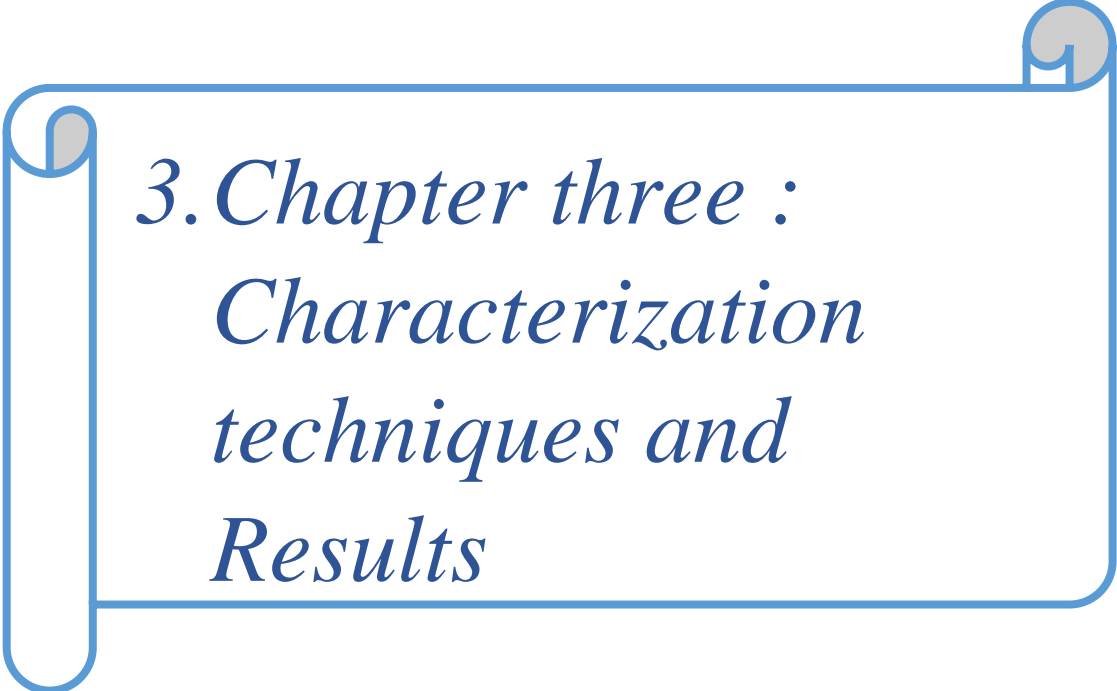

Figure 2.15 Cold Press
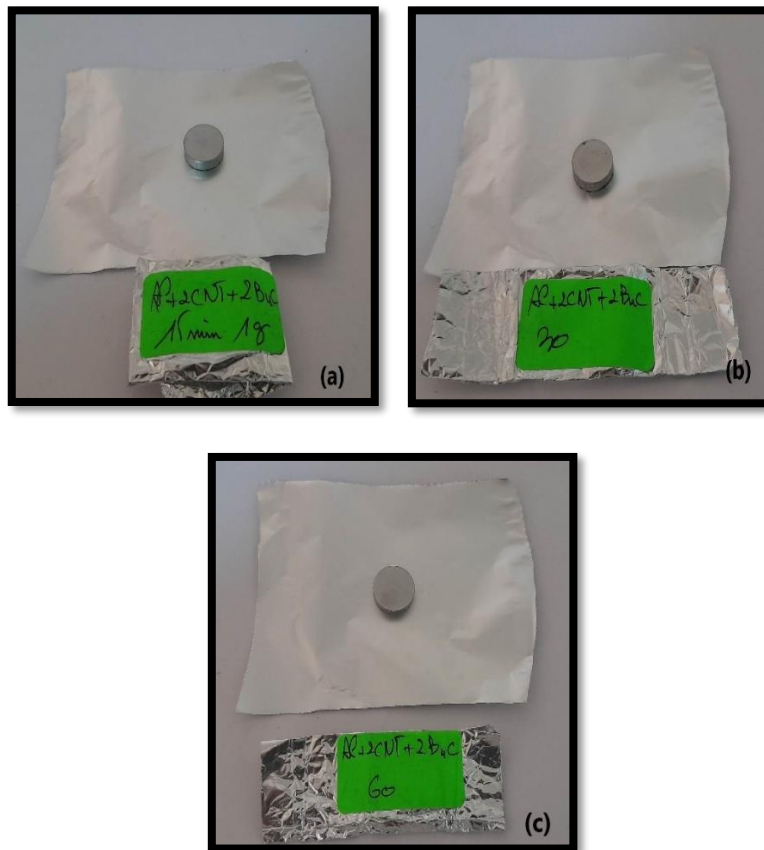
Figure 2.16 *Green compacts obtained by cold consolidation for each processing time (a) 15min, (b) 30min and (c) 60min.*

The specimens obtained for each process time; powders **(Figure 2.14)** and green compacts **(Figure 2.16)** are then analyzed using characterization tools to determine the evolution of their mechanical properties. Using X-Ray diffraction, Scanning Electron Microscopy , and Nanoindentation.

3. Chapter three : Characterization techniques and Results

The evaluation, characterization, and assurance of nanocomposite materials are essential concerns for material scientists, structural engineers, and users. These issues are significant for those who require high-quality nanocomposites in specific applications as aerospace industry. To ensure the durability of advanced nanocomposites, thorough evaluation, and monitoring are necessary. This involves rigorous testing and quality control of nanocomposite products. Accurate assessment and monitoring are also crucial components of this process. When determining the merit of created nanocomposites, retaining the quality of their features is critical.

We will evaluate and classify samples from different processing times of our nanocomposite AL-2w%MWCNTs-2w%B$_4$C using three diagnostic tools: Scanning Electron Microscopy (SEM), X-Ray Diffraction (XRD), and Nanoindentation. The subsequent paragraphs provide an examination of these technologies, along with our resulting discoveries.

3.1   Characterization by Scanning Electron Microscopy (SEM)

The Scanning Electron Microscope (SEM) is a powerful tool utilized across various scientific fields, including materials science, nanotechnology. Its primary function is to produce high-resolution images with detailed information about a sample's surface structure. Scanning a focused beam of electrons across the surface, SEMs create highly magnified images that comprehensively view a sample's topography, morphology, and composition. Moreover, SEMs permit researchers to scrutinize the surface features, textures, and properties of a range of materials, allowing them to gather crucial information about a sample's roughness, grain size, and surface defects. SEM is helpful in studying dispersion of CNTs in the powders of a nanocomposite.

3.1.1   Operating Principle of the SEM

The principle of SEM and diagram of the electron probe formation in SEM are illustrated in **(Figure 3.1)**. Electron microscopes (SEMs) use a beam of electrons to produce high-resolution images of samples at the nanometer scale. The electrons are emitted from a filament and directed into a beam by the electron source, then focused onto the sample surface by lenses in the electron column. Electron microscopes offer various signal types

that can reveal helpful information about the sample, and it is up to the operator to choose which signal to capture. The sample generates secondary (SE) and backscattered (BSE) electron and X-ray signals when exposed to high-energy electrons.

BSE have high energy and are scattered out of the sample, losing only a tiny amount of energy. They originate deep within the sample, a few microns below the surface, interacting strongly with it. Backscattered electrons provide compositional information and lower-resolution images as they are reflected after elastic interactions between the beam and the sample.

Secondary electrons (SE) are particles that originate from within a few nanometers of the sample surface. They have lower energy than the backscattered electrons but are highly sensitive to surface structure, providing topographic information. These electrons are a result of inelastic interactions between the electron beam and the atoms of the sample.

Information about the elemental composition of a sample can be obtained by analyzing the characteristic X-rays produced when electrons hit the sample's surface.

BSE and SE originate from different parts of the sample, with BSE coming from deeper regions and SE from surface regions. This means that they carry distinct types of information. BSE images reveal variances in atomic number, with a higher atomic number appearing brighter in the image. Meanwhile, SE imaging provides more precise surface details[63].
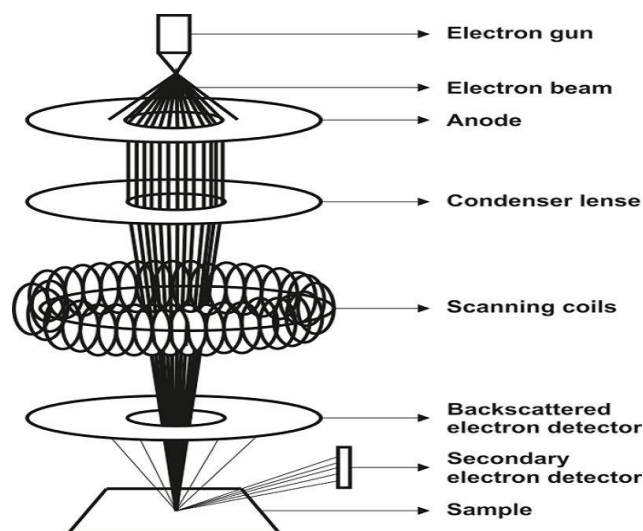
*Figure 3.1 Electron path in scanning electron microscope [64]*

3.1.2 Results and Discussions

In order to understand how the size and shape of particles affect the mechanical performance of Al-2w%MWCNTs-2w%B_4C nanocomposites, we observed the morphology of the particles with a Quanta 650 scanning electron microscope **(Figure 3.2)** equipped with a Tungsten filament (W) to examine the initial samples at (0min) and the final samples after (60min) of mechanical alloying. We used a secondary electron detection mode (EDT) to detect even the most minor surface changes and collect varying amounts of electrons. This provided us with information on the topology of the samples. The used acceleration voltage was 15 kV, and the typical working distance was 10 mm. The micrographs were taken at magnifications ranging from 1200 to 200000.


Figure 3.2 Quanta 650 microscope

The **(Figure 3.3)** shows a SEM image of the initial specimen (Al-2w%MWCNTs-2w%B_4C), used to produce the nanocomposite, showing a significant presence of spherical aluminum particles with an average size ranging from 6 μm to 500 nm. The B_4C ceramic particulates were seen as a blade shape. The as received MWCNTs as were found to be agglomerated due to strong Vander Waal's force of attraction between the CNTs.
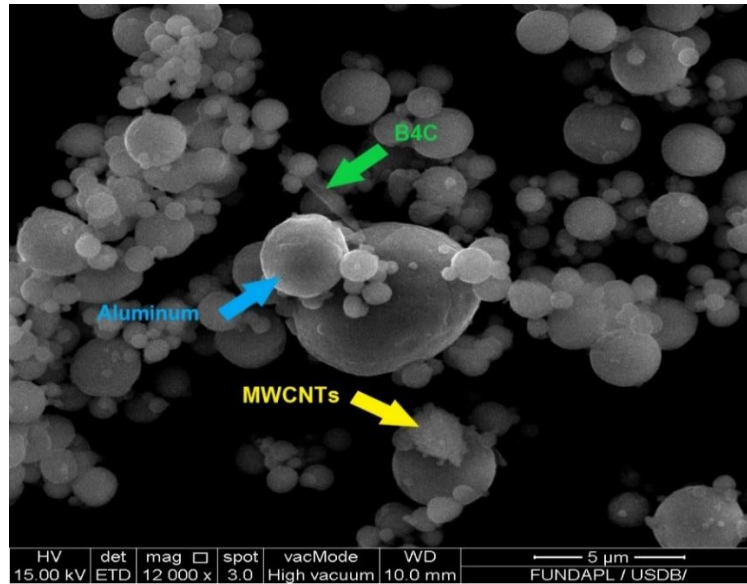
Figure 3.3 Morphology of the initial specimen

After grinding for 60 minutes, the particles' initial form vanished entirely **(Figure 3.4)**. The structure formed due to fragmentation caused by crushing, resulting in a mixture of small and larger particles ranging from 5 μm to 20 μm **(Figure 3.5)**. After repeated collisions between the particles, balls, and vessel walls break down the material into nano-powder through compression, shear, and frictional forces, the specimens were then consolidated by high cold pressure. We observed that Al particles are almost spherical in the initial stage after ball milling and the particles changes into flake like ones, The research article [65] displayed identical results to ours. The reinforcements are barely visible, possibly because the matrix has covered the MWCNTs and B_4C particles. No agglomerations were visible, and this indicates that materials were well mixed together.
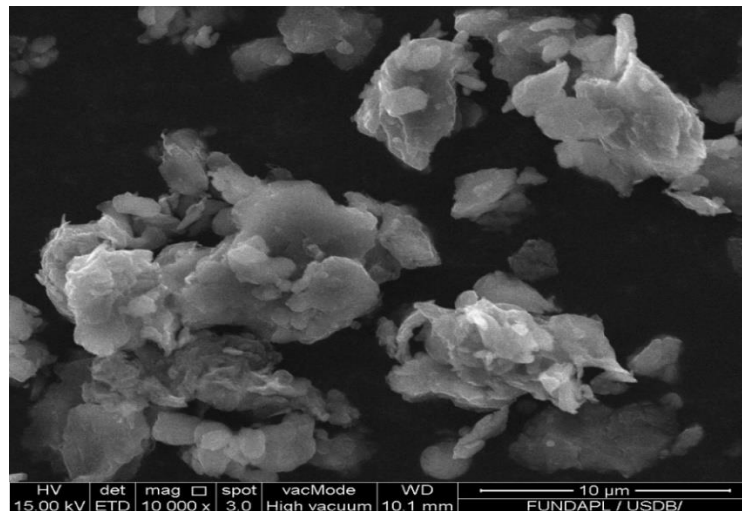

Figure 3.4 Morphology of the specimen after 60min of milling
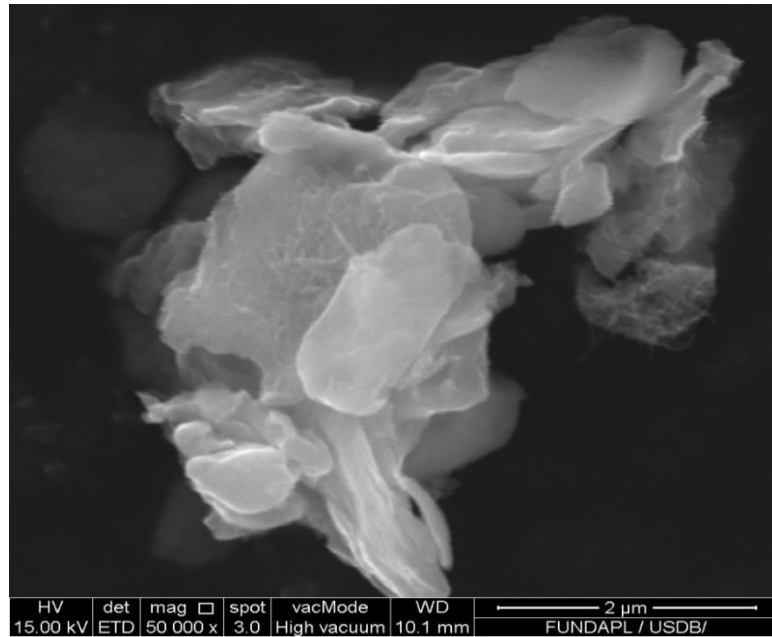
Figure 3.5 Morphology of a particle after 60min of milling with visible MWCNTs

To study the dispersion of the reinforcements within the matrix an EDX analysis which is a chemical technique employed in conjunction with the SEM was done for the two samples at 0 and 60 minutes of milling. **(Figure 3.6)** shows the EDX global analysis results for the initial sample of 96w%Al with 2w%MWCNT and 2w%B4C. The analysis confirms the presence of Aluminium, Oxygen, Boron, and Carbon peaks. And the **(Table 3.1)** shows the percentage of nominal and atomic masses of each element.
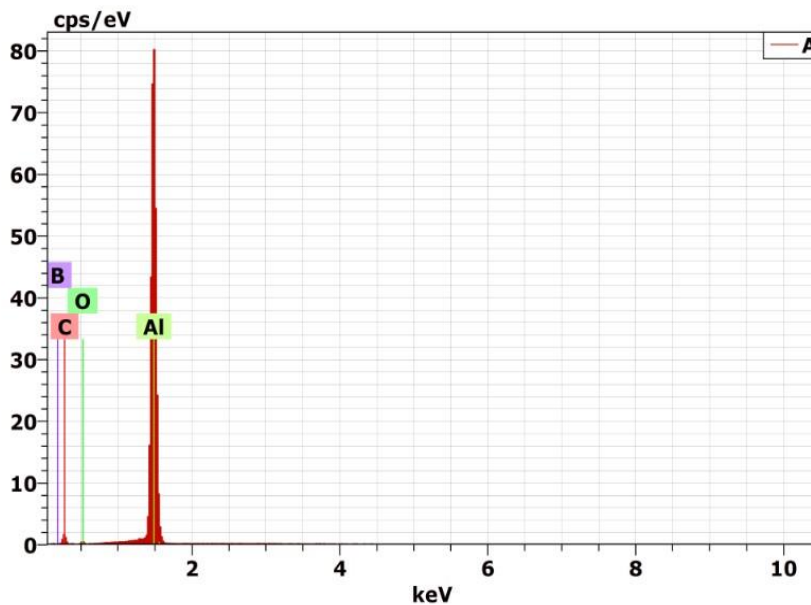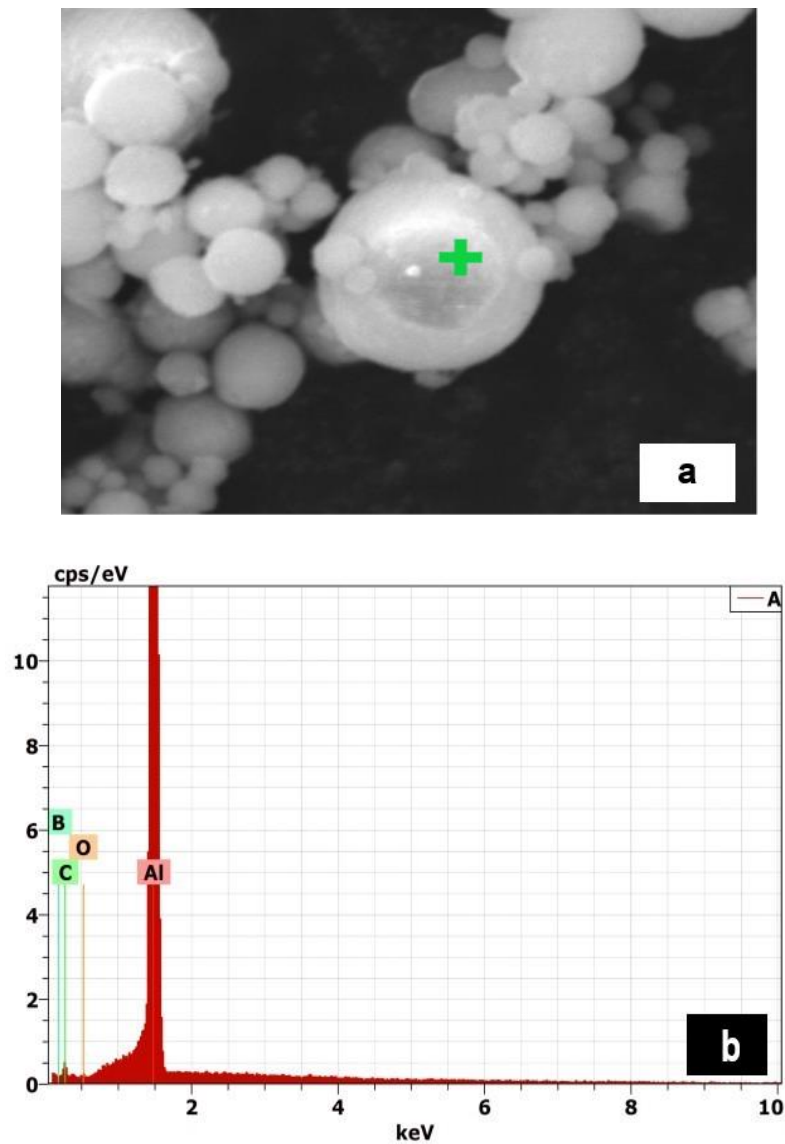

Figure 3.6 Global EDX spectrum of the initial specimen

Table 3.1 *Masses percentage from the global analysis of the elements at 0min*

Elements	Nominal masses%	Atomic masses%
Aluminum	62.97	42.16
Carbon	20.31	30.54
Oxygen	1.19	1.35
Boron	15.53	25.95

A EDX point analysis was performed, and the spectrum in the **(Figure 3.7)** shows the peaks of each element with their masses percentage in the **(Table 3.2)**.
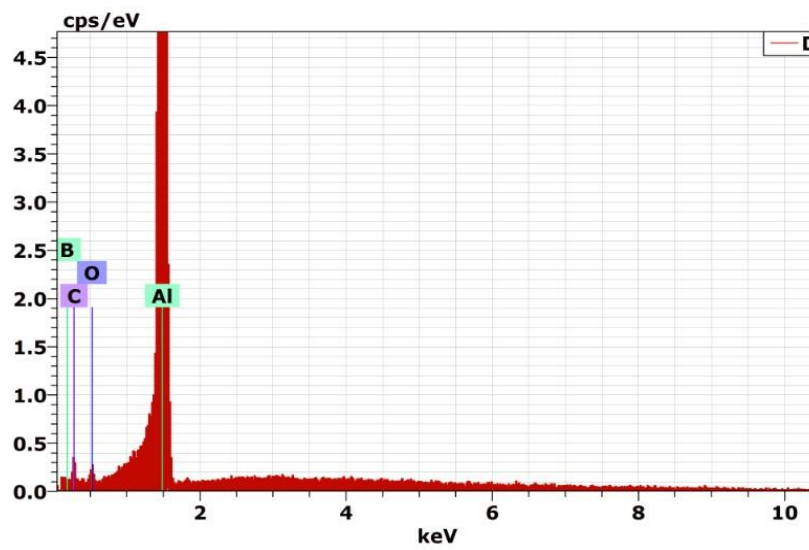

Figure 3.7 *(a) location where point EDX analysis was performed (b)Point EDX spectrum of the initial specimen*

Table 3.2 *Masse percentage from the point analysis of the elements at 0min*

Elements	Nominal masses%	Atomic masses%
Aluminum	74.01	53.99
Carbon	6.94	11.37
Oxygen	0.09	0.11
Boron	18.96	34.52

A global and a point EDX analysis were performed, for the sample milled for 60min and the results are shown respectively below:
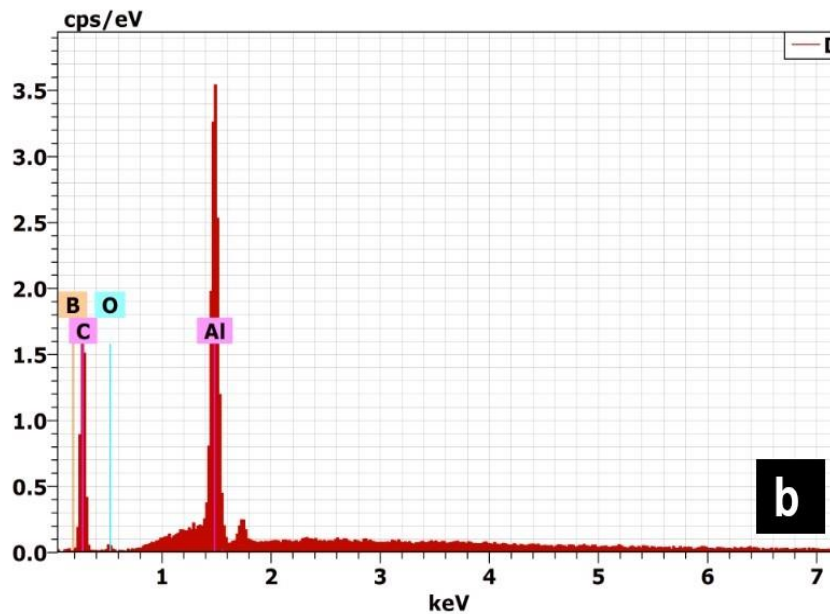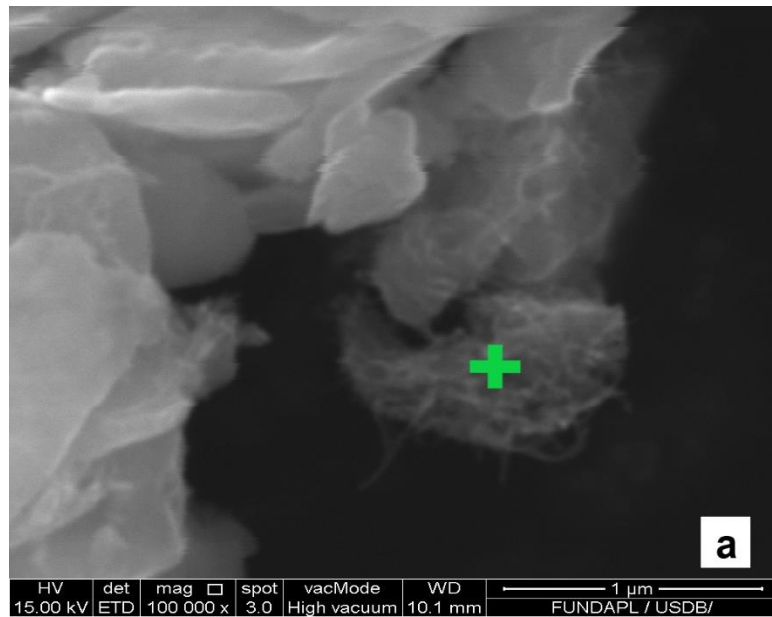

Figure 3.8 *Global EDX spectrum of 60min milled specimen*

Table 3.3 *Masse percentage from the global analysis of the elements at 60min*

Elements	Nominal masses%	Atomic masses%
Aluminum	73.10	52.99
Carbon	6.82	11.10
Oxygen	0.75	0.92
Boron	19.33	34.98

Figure 3.9 *(a) location where point EDX analysis was performed (b)Point EDX spectrum of the 60min milled specimen*

Table 3.4 *Masse percentage from the point analysis of the elements at 60min*

Elements	Nominal masses%	Atomic masses%
Aluminum	72.00	82.45
Carbon	23.15	11.80
Oxygen	1.02	0.88
Boron	3.83	4.87

The EDS analysis confirms that MWCNT and B4C particles are present within the composites. Therefore, these SEM and EDS analysis are evidence of successful incorporation MWCNT particles in Al matrix composites.

3.2   Characterization by X-ray Diffraction (XRD)

XRD is a non-destructive and widely used analytical technique to determine the physical properties of samples, including the phase composition, crystal structure, and orientation. It is a versatile technique that can be used for various materials that consist of tiny crystallites. When examining materials, we can determine their chemical composition and structural type by identifying their 'phase', which can be either single or multiphase. This phase can contain both crystalline and non-crystalline components. We can observe the unique diffraction patterns created by different crystalline phases using an X-ray diffractometer. To identify these phases, we compare the patterns of unknown samples to a reference database, similar to matching fingerprints at a crime scene. The ICDD (International Center of Diffraction Data) which is formerly known as JCPDS; maintains the most comprehensive compound database[66].

3.2.1   Operating Principle of the XRD

X-Ray diffraction is an electromagnetic radiation which is produced by bombarding high energy electrons on any heavy metal; incident electron beam falls on a specimen so we can observe some backscattered, auger and secondary electrons in addition and according to Mosley's law in which every element has its unique signature in the form of **Kα**, each one produces its diffraction so we can also observe X- ray diffraction **(Figure 3.10)** , and the XRD data will be recorded at last; these results can be compared to pre-existing JCPDS files to identify the crystal system of the material used for the investigation.

An electromagnetic radiation can be diffracted by atomic planes only when the half of its wavelength is less than the inter atomic distance $\lambda/2 \leq D$. X-Rays are used over visible light for crystal diffraction because of its shorter wavelength.

The diffraction is the main technique used to identify crystal structures, when a parallel beam diffracted from a single slit it causes a path difference of $d.sin\theta$ and when incident beam is also at an angle θ then the path difference is $2d.sin\theta$.

When atomic planes act as diffraction slits, then the constructive interference is defined by Bragg's Law:

$$2d.sin\theta = n\lambda \ ......(3.1)$$

with d being the inter-planar spacing, θ the half of corresponding angle of diffraction, and λ the wavelength .
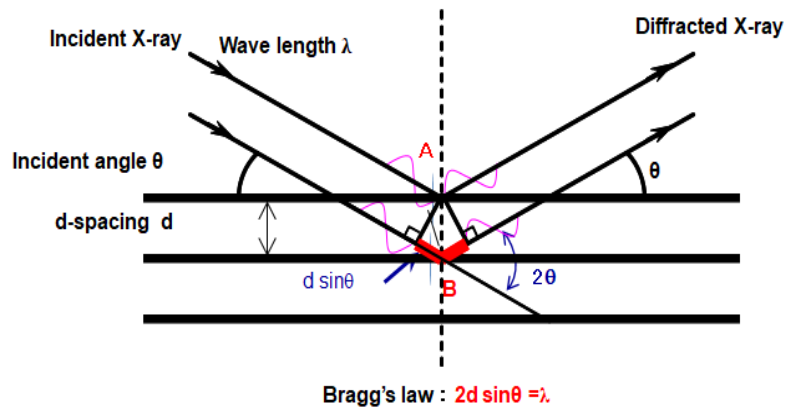
Figure 3.10 *Schematic of an X-ray diffraction principle[67]*

with an X-ray diffractometer the beam of electrons falls on a rotating target and throws out the x-rays generated; a supply of cold water is also provided for keeping target cool. It emits a continuum of x-ray , but we want a particular **Kα**, wavelength. Earlier some filters were used (thin Ni in case of Cu) nowadays monochromators are used , like quartz crystal. Finally, the x-rays fall on the sample and detector containing photomultiplier tube detects it. And from the data recorded we can study the evolution of the phases from detecting:

- Peak Position : all planes diffract coherently at an angle where Bragg's law holds good, the position of a peak determines the inter- planar spacing family of planes.
- Peak Intensity : the intensity of a peak depends on the position of atoms within a unit cell, the superposition of all constructive and destructive contribution which is obviously guided by the position of atoms.
- Peak Width : width of a peak basically depends on two factors crystallite size and lattice strain

3.2.2 Results and Discussions

3.2.2.1 Phase Identification Procedure

We analyzed the powders Al-2w%MWCNTs-2w%B$_4$C produced during three different mechanical grinding times (15min, 30min, and 60min) using an X-ray diffractometer to study their structure. After processing the XRD spectra, we determined the powder crystallinity, phase identification, lattice parameter, mean crystallite size using HighScore plus crystallographic analysis software and Origin graphical data analysis software.

➢ Determination of the Background

To analyze diffractograms, the first step is to identify the background noise **(Figure 3.11)**. This is crucial, and removing it affects the position and shape of the peaks. The recommended values for granularity and bending factor are 23 and 4, respectively, which will generate a green line representing experimental data on the diffractogram. These values can be adjusted for better results, but using the same values for all samples is essential to ensure comparability. It is worth noting that these values can also impact the calculation of crystallite size.
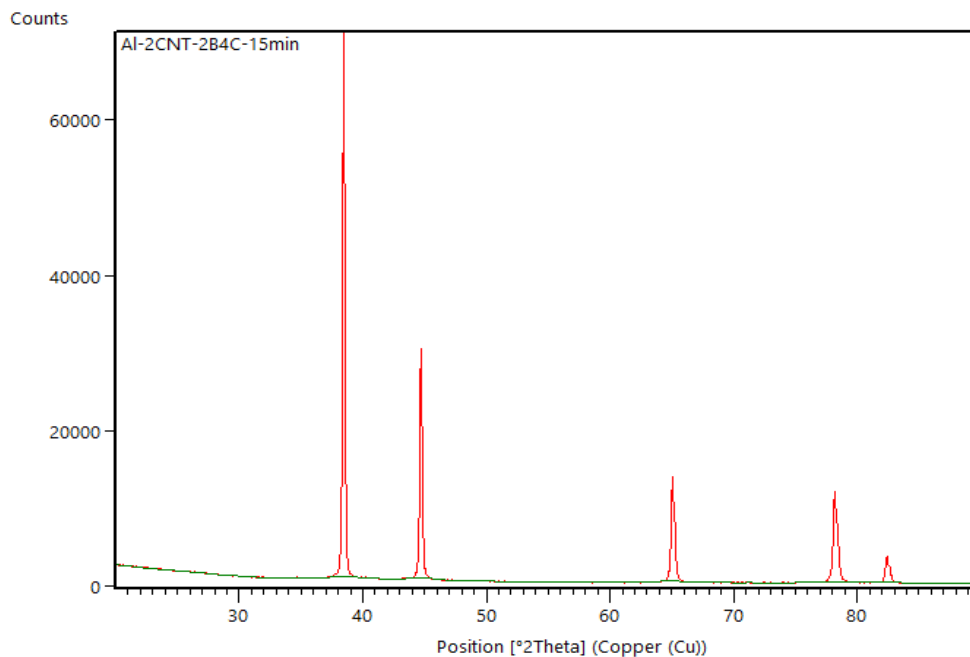

Figure 3.11 *Determination of the background*

➢ Search Peaks Step

This step helps determine the position of diffractogram peaks and estimate their width and intensity. To obtain accurate peaks, several parameters must be set:

The "significance" of a peak on the "search peak" window represents the surface of the second derivative. A peak with a low significance value may be mistaken for background noise.

The "Tipwidth" is the distance between the points of peak deflection or the width of the peak's base. Its value must exceed or equal the "maximum tip width."
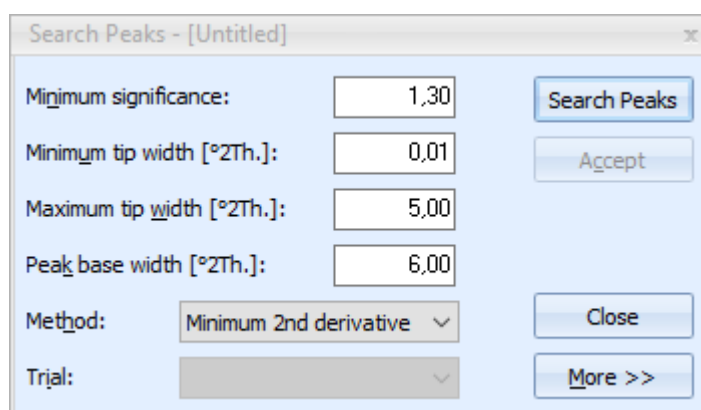
Figure 3.12 *Parameters established for peak searches*

After clicking "search peaks," a blue line appears on the diffractogram, representing the calculated diffractogram. A verification step follows this procedure to ensure that each peak identified on the graph corresponds to a peak on the spectrum and that all peaks have been accounted for and identified.

We took the sample milled for 15 minutes as an example.
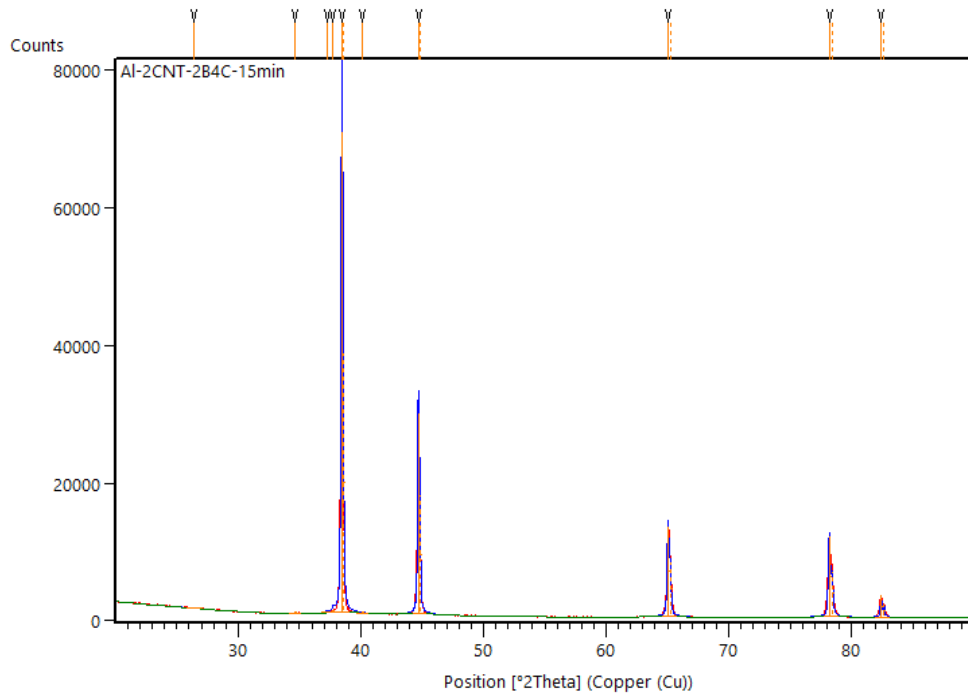
Figure 3.13 The calculated diffractogram to identify peaks of the Al-2CNTs-2B₄C 15min

➢ Create a profile of the simulated peaks by "fit profile"

The best approach to perfecting the peak profile for the simulated diffractogram is to select the "fit profile" option multiple times until there is no discrepancy between the calculated blue line and the red line from the experimental diffractogram.
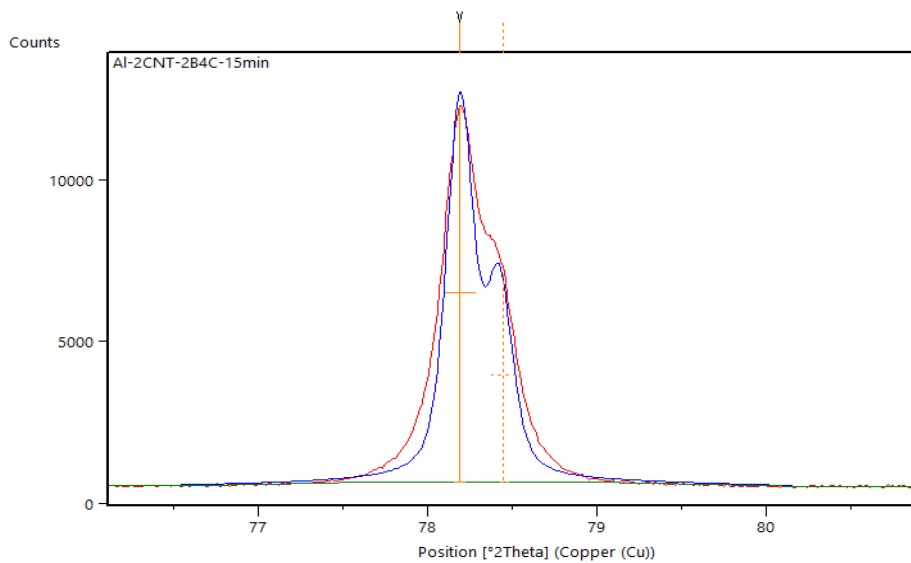

Figure 3.14 Before fitting the profile of the most intense peak in the Al-2CNTs-2B₄C (15min)
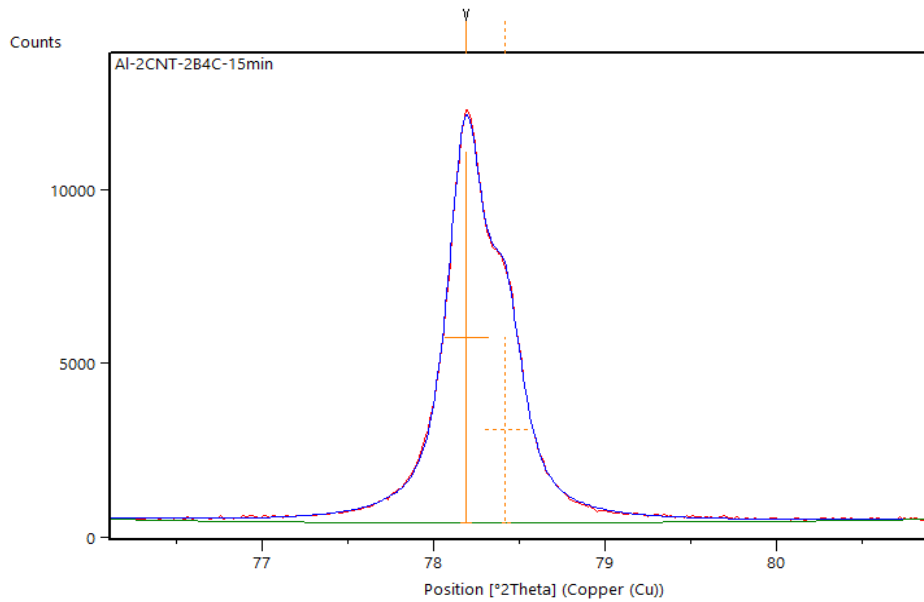
Figure 3.15 *After fitting the profile of the most intense peak in the Al-2CNTs-2B$_4$C (15min)*

➢ Phases Identification

Our identification process involves a two-step approach. Firstly, we search our database for possible matches by conducting a search. Then, we compare these matches with the diffractogram to ensure they are accurate, known as a "search match". We used aluminum, boron, and carbon being the elementary powder for our elaboration.
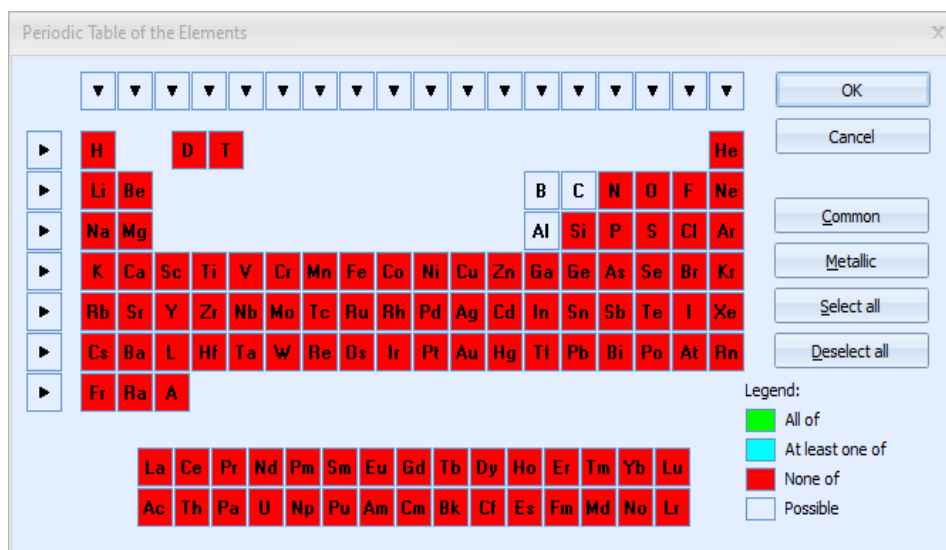
Figure 3.16 *Periodic Table containing all the elements available for selection.*

After selecting viable raw materials, the spectrum obtained from the test sample is compared to all catalogued sheets in order to generate a selection of likely phase compounds. By inspecting the diffraction peaks of possible phase compounds of the diffractogram, we can recognise the particular phases present. By these means, we have identified every phase found in the nanocomposite materials Al-2w%MWCNTs-2w%B$_4$C for all the test samples each one with a different milling time. We can easily identify the aluminum peaks, however, the low concentration of the reinforcements making them challenging to identify their peaks, we can barely identify the B4C peaks but any peaks of CNTs were visible. Similar observation was reported by Basariya et al [68] where they could observe peaks related to aluminium only but none related to CNTs.

3.2.2.2 The present phases in Al-2w%MWCNTs-2w%B$_4$C nanocomposites

> AL-2w%MWCNTs-2w%B4C after 15min of milling

We identified the phases present in the 15 minutes milled sample **(Figure 3.17)**. We observed that the aluminum diffraction had all peaks with a face-centered cubic structure at positions of 2θ = 38.4282°, 44.6768°, 65.0534°, 78.1865°, 82.3936° with Miller indices of (111), (002), (022), (113), and (222) respectively. The boron carbide had a hexagonal structure at positions of 2θ = 34.7474°, 37.6242°, 40.1300° with Miller indices of (104), (021), and (003) respectively.

The Miller indices allow us to quantify and specify the crystal planes, a crystal plane or a lattice plane is the plane which passes through the crystal and intersects lattice.
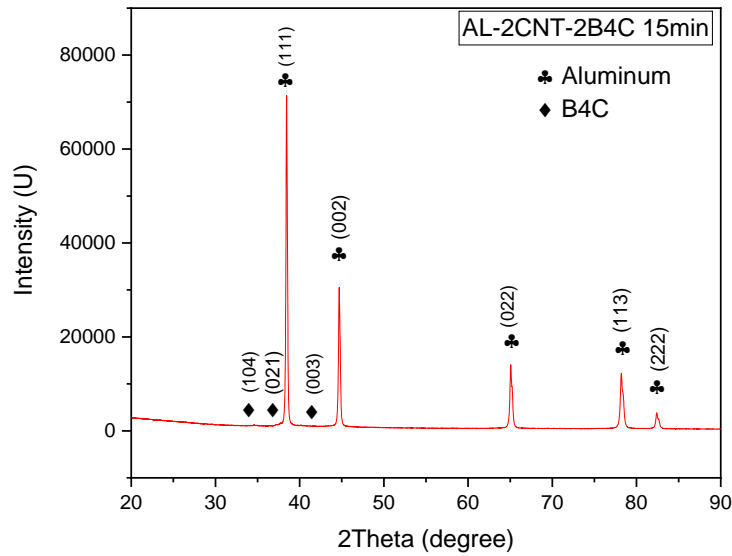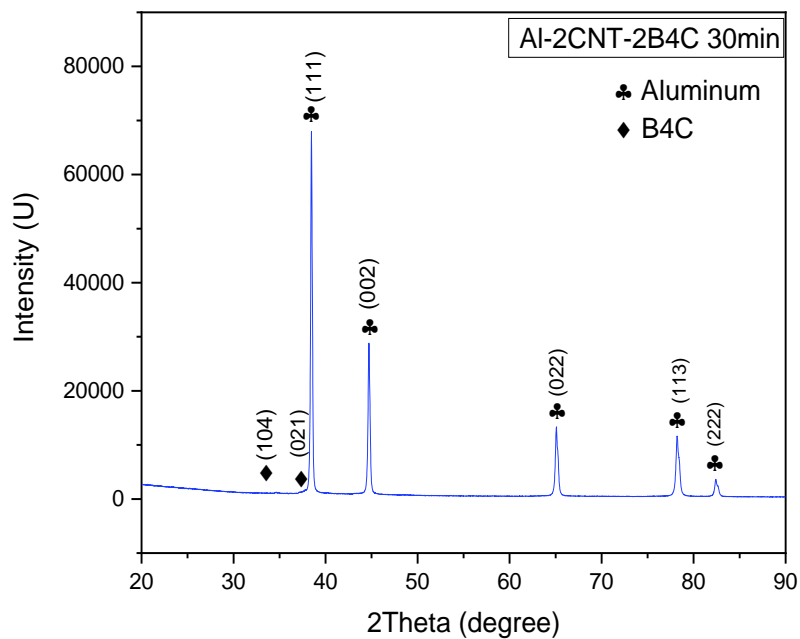
Figure 3.17 Phases and Miller indices of the sample milled for 15 min

➢ AL-2w%MWCNTs-2w%B₄C after 30min of milling

In the sample milled for 30 min **(Figure 3.18)**, we observed that the aluminum diffraction had all peaks with a face-centered cubic structure at positions of $2\theta = 38.4372°$, 44.6858°, 65.0625°, 78.1957°, 82.4027° with Miller indices of (111), (002), (022), (113), and (222) respectively. The boron carbide had a hexagonal structure at positions of 2θ = 34.614° and 37.331° with Miller indices of (104) and (021) respectively.

➢ AL-2w%MWCNTs-2w%B4C after 60min of milling

In the sample milled for 60 min **(Figure 3.19)**, we observed that the aluminum diffraction had all peaks with a face-centered cubic structure at positions of $2\theta = 38.3795°$, 44.6269°, 64.992°, 78.1289°, 82.3347° with Miller indices of (111), (002), (022), (113), and (222) respectively. The boron carbide had a hexagonal structure at positions of 2θ = 34.8663°, 37,7176° with Miller indices of (104) and (021) respectively.

70

***Figure 3.18*** *Phases and Miller indices of the sample milled for 30 min*
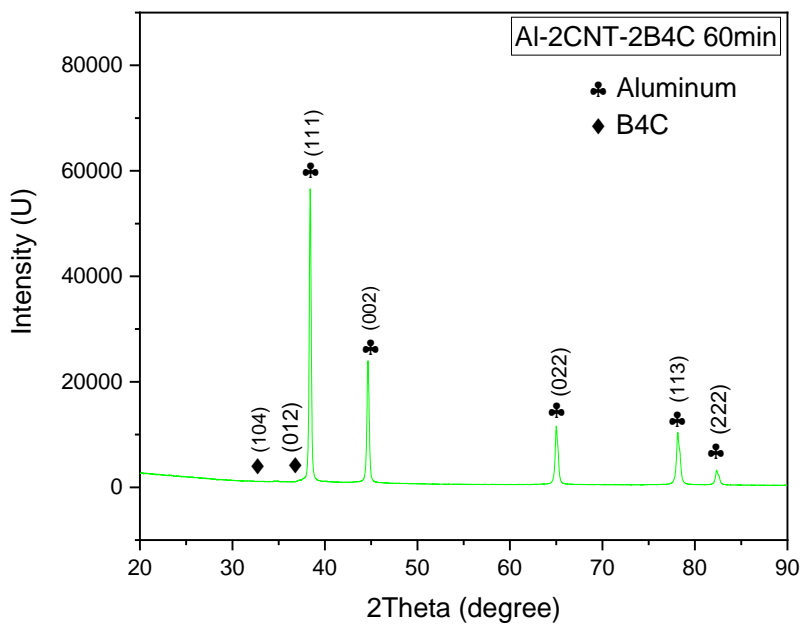
Figure 3.19 *Phases and Miller indices of the sample milled for 60 min*

3.2.2.3 The phases evolution of the nanocomposite

To observe the evolution of peaks and phases in AL-2w%MWCNTs-2w%B$_4$C we superposed the XRD diffractogram for each specimen (15min, 30min, and 60min) **(Figure 3.20)**. As the crushing time increased, we observed a gradual decrease in peak intensity, peaks shifting to the small Bragg's angles and additionally we noticed widening of the peaks.

Increasing the grinding time reduces the intensity of the diffraction peaks indicating the impact of crushing on the powders. After 30 min of grinding, the B4C (003) peak disappears, and after 60 min of grinding, a shift of the aluminum peaks towards the small Bragg angles, and their widening is observed. This progressive shift of the peaks is attributed to the increase in the interarticular distance, and the primary stress undergone by the aluminum during grinding. The widening of the aluminum peaks indicating a continuous decrease in grain size and to the numerous internal stresses (micro distortions) introduced into the crystallin network during grinding. It is important to note that so far, the carbon phase has not been identified, and this is due to the small number of carbon nanotubes used and the very low intensity of its diffraction; according to the HighScore software, after 60 min, the aluminum has maintained its initial crystalline structure of face-centered cubic, on the other hand, the aluminum has covered a considerable part of the carbon nanotubes. This leads us to conclude that using medium grinding energy maintains the initial shape of the elements while synthesizing them with homogenization. In addition, the X-ray diffraction studies showed that no undesirable phases were formed after ball milling. According to (Gowda et al., 2018)[69], the formation of carbides/oxides usually results in the poor mechanical properties of composites.
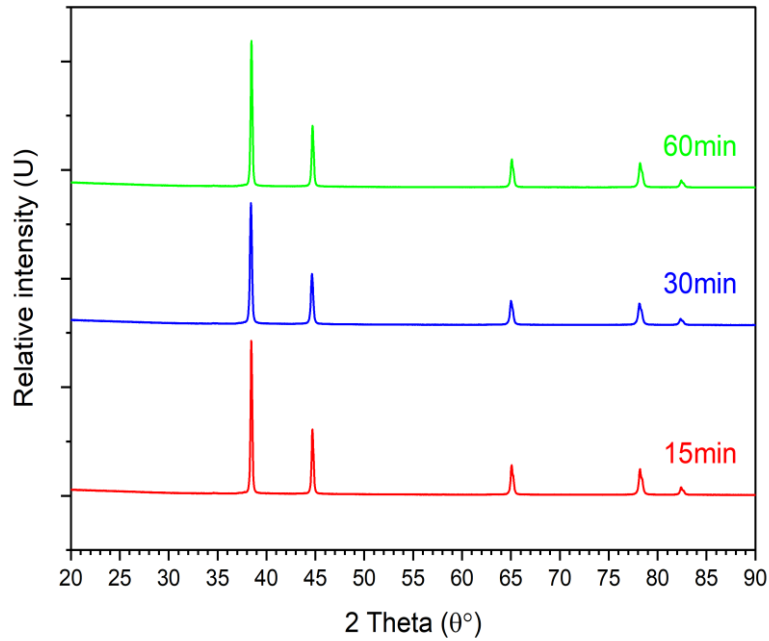
Figure 3.20 *Diffractogram pattern of the three samples*

3.2.2.4   Evolution of the lattice parameter

We used the cubic lattice relationship to calculate the lattice parameter, a(Å), for all samples. This involved considering the most intense peak and applying the formula.

$$a = d_{hkl} \sqrt{h^2 + k^2 + l^2} \ \ldots\ldots(3.2)$$

With:

a : lattice parameter

d_{hkl} : interreticular distance

h, k, l : Miller indices

The **(Figure 3.21)** shows how the lattice parameter changes over time as the grinding process takes place. The value starts at 4.051 Å and increases to 4.059 Å after 60 minutes of grinding. There are two stages in the evolution of the lattice parameter. Firstly, within the first 15 minutes of grinding, the lattice parameter decreases. This suggests the existence of an ordered structure, which reduces the lattice parameter. Secondly, after 30 minutes of grinding, the parameter increases. This indicates that carbon nanotubes and boron carbide are diffusing in the aluminum matrix.

73
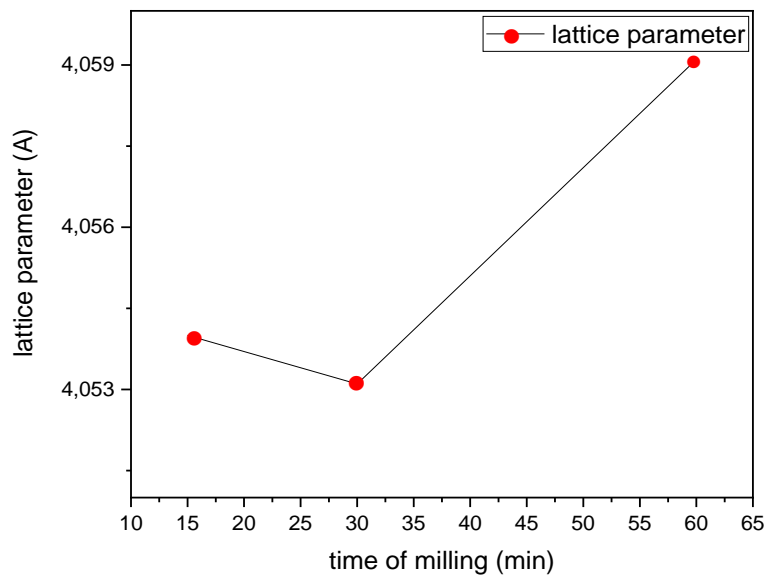
Figure 3.21 *Evolution of the lattice parameter*

The **(Figure 3.22)** shows that as the lattice parameter increases, the diffraction peaks shift towards smaller angles.
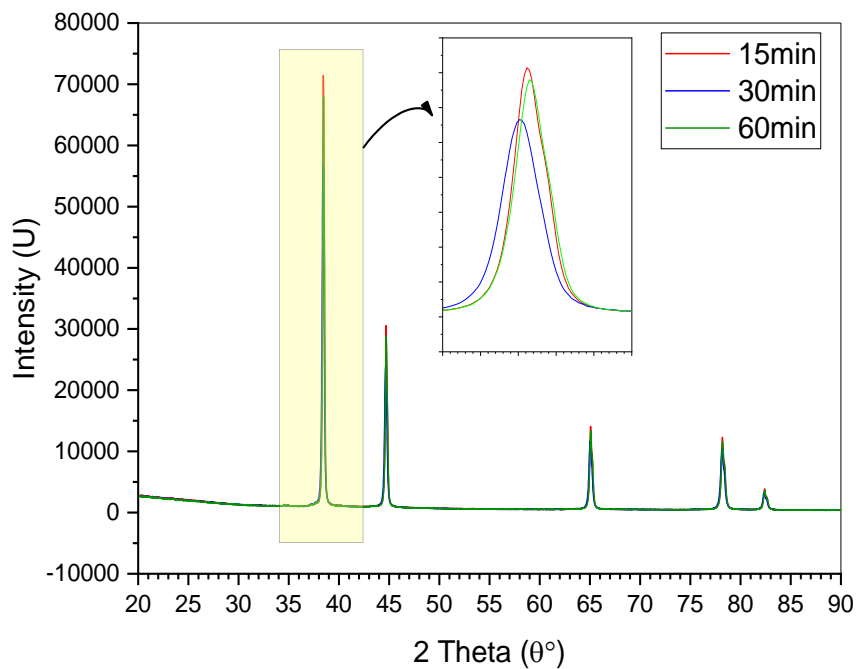
Figure 3.22 *peak shifting as a function of grinding time*

3.2.2.5 Evolution of the crystallite size during the milling time

The size of a coherently diffracting piece of a crystal (crystallite) in the XRD pattern can be calculated by Scherrer's formula:

$$D = \frac{k\lambda}{\beta \cos\theta} \quad \ldots\ldots(3.3)$$

With:

k = 0.94

λ: wavelength

β: full width at half maximum peak

θ: half of the corresponding peak angle

The software application 'Origin' helped us determine the precise location of each sample's intense peaks (2θ) and permitted us to estimate their full width at half maximum (FWHM). In **(Figure 3.23)**, we can see how the size of the crystallites (measured in nanometers) changes over time as the material is ground. As we grind the material for extended periods, the average size of the crystallites decreases. The average size goes from 403.881nm for the aluminum phase to 347.922nm.
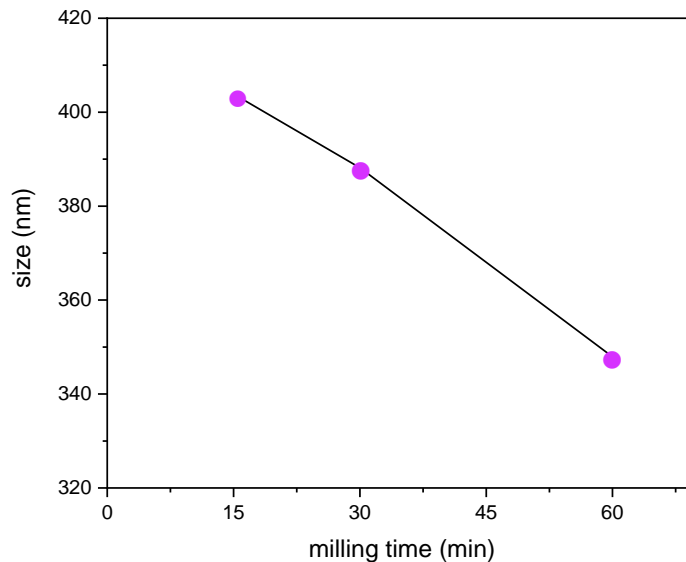
Figure 3.23 *Evolution of the crystallite size*

3.3 Characterization by Nanoindentation

Nanoindentation, also called instrumented indentation testing, is a technique used to measure the hardness of materials. This method is crucial in materials testing, as it enables the evaluation of properties such as the elastic indentation modulus E_{IT} and the indentation hardness H_{IT}, among others, for both plastic and elastic materials. Nanoindentation differs from traditional methods like Vickers or Martens as it provides precise, depth-dependent measurements of multiple material-specific parameters rather than just a single value[70].

3.3.1 Operating Principle of Nanoindentation

The process of nanoindentation **(Figure 3.24)** requires the use of a diamond indenter with high precision to penetrate a sample and measure both the load and depth of penetration. This generates a load-depth curve, which can be recorded during the indentation's loading and unloading stages. The material's modulus of elasticity governs the slope of the unloading curve at maximum load. The loading-unloading curve can provide valuable information about the material's elastic and plastic work and yield strength. This technique is highly advantageous since it can be performed on even the smallest samples and features, including those as small as a human red blood cell. The load and displacement are measured with exceptional accuracy and resolution during the indentation process, and recent advancements in instrumentation and sensing capabilities have made it possible to achieve a load resolution of nano-Newtons and depth resolution in nanometers[71].
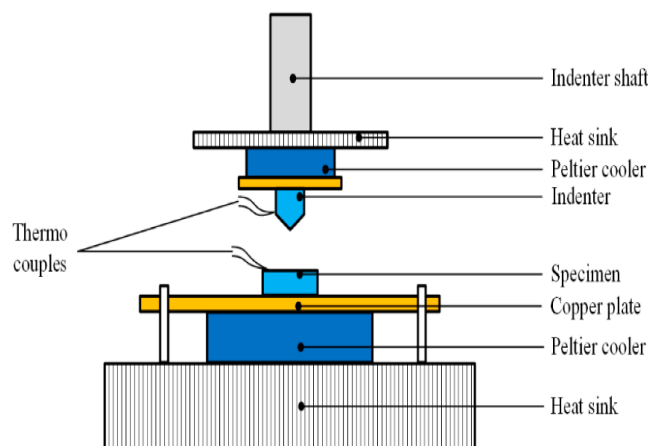
Figure 3.24 Nanoindentation setup[72]

3.3.2 Results and Discussions

The more metal is made up of fine grains, the harder it is. Within a classic metal, there are dislocations which are structural defects joining the aggregates. When stress is exerted on the metal, this causes the dislocations to move, and the metal deforms. In nanomaterials, the fraction of dislocations is very small compared to that of grain boundaries. In the absence of these defects, resistance to deformation becomes greater.

After applying the Martens hardness test method, with a load of 1N for 10s of application time.

Table 3.5 Results of the hardness test for the different milling time

	HV1		
	15	**30**	**60**
1	77	90	119
2	86	97	135
3	81	80	124
4	84	105	124
5	94	96	129

the results shown in **(Figure3.)** reveal the increase in HV1 values as a function of grinding time. The hardness of the nanocomposite (Al-2w%MWCNTs-2w%B_4C) increases from 84.4 for the sample ground for 15 min to 126. 2 for the sample ground for 60 min. This increase is largely attributed to the incorporation of boron carbide, It has been proven in the (Alizadeh et al., 2015) article[73] that when boron carbide particles are absent (in the Al-CNT sample), the hardness decreases instead of increasing. This can be explained by the weak bonding between the carbon nanotubes (CNTs) and the aluminum matrix, resulting in porosity and inadequate bonding between particles and the matrix. This is due to clustering and segregation at the grain boundaries. and to the reduction of the crystallites size under the effect of grinding because, as seen previously through the Hall-Petch equation, the reduction in grain size increases the minimum stress required to deform the material plastically.
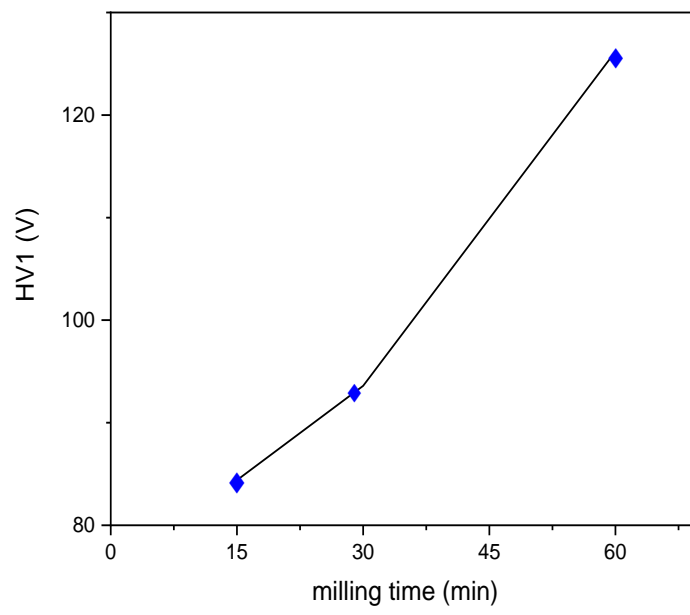
Figure 3.25 *Evaluation of the hardness function of the milling time*

Conclusion
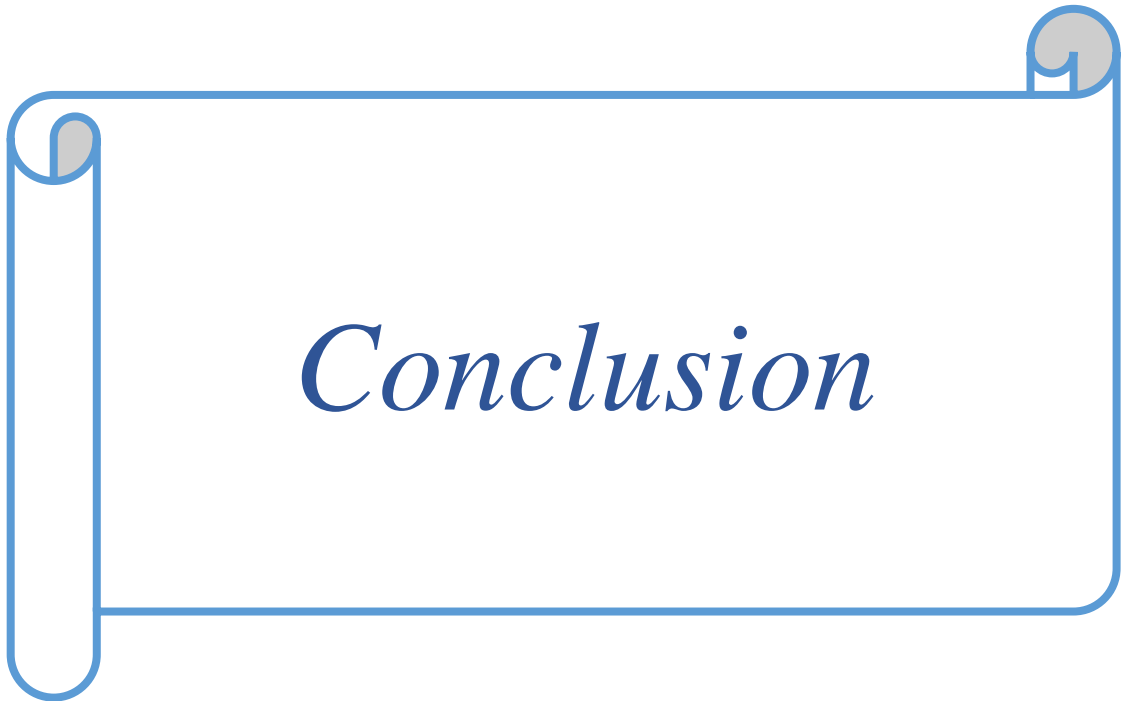
Using mechanical alloying, we successfully synthesized a hybrid aluminum matrix reinforced with B_4C and MWCNTs. The dispersion of CNTs in the metal matrix is affected by attractive van der Waals forces. We adopted mechanical alloying to achieve a homogenous distribution of multiple reinforcements, namely B_4C and CNTs, within the commercial purity aluminum powder. This process was carried out in a planetary ball mill for up to 60 minutes, and we systematically studied the milling process by taking small amounts of powder from three specimens at different milling times of 15, 30, and 60 minutes respectively.

To characterize the MWCNT and B_4C particles dispersed in Al matrix composites, we used SEM with EDX, XRD, and Nanoindentation. The EDS analysis confirms the presence of B_4C and carbon nanotubes within the composites. The SEM structures are evidence of the successful incorporation of hybrid Al-2w%B_4C-2w%MWCNT nanocomposites. The XRD pattern confirms the Al and B_4C peaks using JCPDS files. Our goal has been achieved, as the nanocomposites have undergone a considerable reduction in grain size from 403.881nm to 347.922nm, resulting in a significant increase in hardness from 84.4 HV to 126.2 HV in 60 minutes of milling, according to the results of Nanoindentation analysis. Although there has been minimal crushing time, new phases have not formed.

To conclude, the potential of Al-MWCNTs-B_4C nanocomposites for progressively manifesting capabilities in the fabrication of aircraft structures has been created. Discoveries from this study increase awareness of the different capacities and features of CNTs and B_4C reinforcements. Consequently, concerted efforts must be made to expand feasibility knowledge, realize robust longevity, and establish how effectively nanocomposites can deal with actual aerospace practices. Overall, if progress continues, incorporating those nanocomposites ought to do an excellent service in the aeronautic industry domain, tending to planes exhibiting advanced strength, efficacy, and high-level security.

References

[1]   'Composites Used in the Aerospace Industry', AZoM.com, Feb. 13, 2013. https://www.azom.com/article.aspx?ArticleID=8152 (accessed Jun. 14, 2023).

[2]   R. Deo, (2003) "Low-Cost Composite Materials and Structures for Aircraft Applications,"

[3]   AERO   -   Boeing   787   from   the   Ground   Up.   (n.d.). https://www.boeing.com/commercial/aeromagazine/articles/qtr_4_06/article_04_2. html

[4]   SAE Media Group, "Simulating Thermal Expansion in Composites with Expanded Metal Foil for Lightning Protection," Mobility Engineering Technology, Jul. 05, 2016. (accessed Jun. 14, 2023).

[5]   Mellema, G. (2012, August 3). Advanced Composites & Helicopters. Aviation Pros.

[6]   B. Castanié, (2016) . Composite structures in aeronautics: past, present and future.

[7]   Cmsadmin. (2022, February 4). NH90 NFH Nato Frigate Helicopter. Airforce Technology.   https://www.airforce-technology.com/projects/nh90-nfh-asw/(accessed Jun. 14, 2023).

[8]   William D. Callister (2008). Fundamentals of Materials Science and Engineering.

[9]   Lorella Ceschini & Arne Dahle & Manoj Gupta & Anders Eric Wollmar Jarfors & S. Jayalakshmi & Alessandro Morri & Fabio Rotundo & Stefania Toschi & R. Arvind Singh, (2017). Aluminum and Magnesium Metal Matrix Nanocomposites.

[10]   Hu, H., Onyebueke, L., & Abatan, A. O. (2010). Characterizing and Modeling Mechanical Properties of Nanocomposites-Review and Evaluation. Journal of Minerals and Materials Characterization and Engineering,

[11]   Collective, (2013). Composite materials handbook. Volume 4, Metal matrix composites

[12]   'Natarajan N, Krishnaraj V, Davim JP.(2015). Metal Matrix Composites: Synthesis, Wear Characteristics, Machinability Study of MMC Brake Drum.

[13] Florea, R. M. (2017). Understanding AlN Obtaining Through Computational Thermodynamics Combined with Experimental Investigation. *IOP Conference Series*.

[14] *'classification of composite materials based on matrix'. https://www.pdfprof.com/PDF_Image.php?idt=14672&t=27#searchs. (accessed Jun. 18, 2023).*

[15] *H. Kalidasu and M. Beri, (2021) 'Wear performance investigation of metal matrix composites.*

[16] *Ding, W., Cheng, Y., Chen, T., Zhao, X., & Liu, X. (2020). Research Status and Application Prospect of Aluminum Matrix Composites. Research and Application of Materials Science.*

[17] *Melendrez Armada & Daniel Alfonso & Proctor & John Edward & Vijayaraghavan & Aravind (2016). An introduction to graphene and carbon nanotubes.*

[18] *Arvind Agarwal & Srinivasa Rao Bakshi & Debrupa Lahiri (2010). Carbon Nanotubes: Reinforced Metal Matrix Composites (Nanomaterials and their Applications)*

[19] *Michael J. O'Connell (2006) 'Carbon nanotubes: properties and applications.*

[20] *Iijima, S. (1991). Helical microtubules of graphitic carbon. Nature.*

[21] *Goyal, R. N. (2017). Nanomaterials and Nanocomposites.*

[22] *Figure 1. Structures of selected allotropes of carbon. (n.d.). ResearchGate. https://www.researchgate.net/figure/Structures-of-selected-allotropes-of-carbon_fig1_288835294.(accessed May 13, 2023)*

[23] *Ado Jorio & Gene Dresselhaus & Mildred S. Dresselhaus (2008). Carbon Nanotubes: Advanced Topics in the Synthesis, Structure, Properties and Applications.*

[24] *Magrez, A., Seo, J. K., Smajda, R., Mionić, M., & Forró, L. (2010). Catalytic CVD Synthesis of Carbon Nanotubes: Towards High Yield and Low Temperature Growth. Materials.*

[25] Sie Chin Tjong (2009). *Carbon Nanotube Reinforced Composites Metal and Ceramic Matrices.*

[26] Baig, Z., Mamat, O., & Mustapha, M. (2016). *Recent Progress on the Dispersion and the Strengthening Effect of Carbon Nanotubes and Graphene-Reinforced Metal Nanocomposites: A Review. Critical Reviews in Solid State and Materials Sciences.*

[27] N. Wu,(2012) *'Carbon Nanotubes Reinforced Nano-Composite Materials and Their Application in Aeronautics Engineering', J. Aeronaut. Aerosp. Eng., vol. 01, no. 04.*

[28] H. K. Wei, Y. J. Zhang, and H. Y. Gong,(2009) *'Preparation and characteristics of multiwalled carbon nanotubes reinforced boron carbide composites'.*

[29] Thevenot, F. (1990) *Boron Carbide—A Comprehensive Review. Journal of the European Ceramic Society, 6, 205-225. - References - Scientific Research Publishing. (n.d.).*

[30] Zhang, W. (2021). *A review of tribological properties for boron carbide ceramics.*

[31] Kuliiev, R., Orlovskaya, N., Hyer, H., Sohn, Y., Lugovy, M., Ha, D., Radovic, M., Castle, E. G., Reece, M. J., Sasikumar, P. V. W., Conti, L., Graule, T., Kuebler, J., & Blugan, G. (2020). *Spark Plasma Sintered B4C—Structural, Thermal, Electrical and Mechanical Properties. Materials.*

[32] Biçer, H., Akdogan, E., Şavklıyıldız, İ., Haines, C. J., Zhong, Z., & Tsakalakos, T. (2020). *Thermal expansion of nano–boron carbide under constant DC electric field: An in situ energy dispersive X-ray diffraction study using a synchrotron probe. Journal of Materials Research.*

[33] Li, X., Wu, J., Tang, C., Zhoukun, H., Yuan, P., Sun, Y., Lau, W., Zhang, K., Mei, J., & Huang, Y. (2019). *High temperature resistant polyimide/boron carbide composites for neutron radiation shielding. Composites Part B-engineering, 159, 355–361. https://doi.org/10.1016/j.compositesb.2018.10.003*

[34] Today, B. (2021, November 8). *Boron: The Holy Grail Of Aerospace And Defense | Borates Today.*

[35] B. Matchen,(1996) *'Applications of Ceramics in Armor Products'.*

[36] . Borgonovo, C., & Apelian, D. (2011). *Manufacture of Aluminum Nanocomposites: A Critical Review Materials Science Forum, 678, 1–22.*

[37] Sanaty-Zadeh, A. (2012). *Comparison between current models for the strength of particulate-reinforced metal matrix nanocomposites with emphasis on consideration of Hall–Petch effect. Materials Science and Engineering A-structural Materials Properties Microstructure and Processing, 531, 112–118.*

[38] Li, H., Zhao, S., Ou, Y., & Lai, Y. (2016). *Synthesis, microstructure, and mechanical properties of in situ TiB2/Al-4.5Cu composites. Science and Engineering of Composite Materials, 25(3), 453–462.*

[39] W. H. Yu, S. L. Sing, C. K. Chua, C. N. Kuo, and X. L. Tian.(2019) *'Particle-reinforced metal matrix nanocomposites fabricated by selective laser melting: A state of the art review', Prog. Mater. Sci., vol. 104, pp. 330–379.*

[40] Camargo, P. H. C., Satyanarayana, K. G., & Wypych, F. (2009). *Nanocomposites: synthesis, structure, properties and new application opportunities. Materials Research-ibero-american Journal of Materials, 12(1), 1–39.*

[41] Sahu, M. K., & Sahu, R. K. (2018). *Fabrication of Aluminum Matrix Composites by Stir Casting Technique and Stirring Process Parameters Optimization. InTech eBooks.*

[42] G. Chatel and J. C. Colmenares,(Jan. 2017) "Sonochemistry: from Basic Principles to Innovative Applications," *Topics in Current Chemistry*, vol. 375, no. 1,

[43] *'The Temperature of Cavitation | Science'. https://www.science.org/doi/10.1126/science.253.5026.1397(accessed May 28, 2023)*

[44] Bang, J. H., & Suslick, K. S. (2010). *Applications of Ultrasound to the Synthesis of Nanostructured Materials. Advanced Materials, 22(10), 1039–1059.*

[45] *'Cold-Chamber Die Casting | Die Casting Process | Die Casting', Dynacast. https://www.dynacast.com/en/specialty-die-casting/die-cast-process/cold-chamber/die-casting(accessed Jun. 16, 2023).*

[46] Matli, P. R., Manakari, V., Parande, G., Kotalo, R. G., & Gupta, M. (2022). *Processing, microstructure and mechanical response of a shell (Magnesium) – Core (Magnesium + Lithium) hybrid composite. Materials Today: Proceedings, 62, 471– 474.*

[47] *Fig. 2. Schematic of DMD process set up with simultaneous wire and. . . (n.d.). ResearchGate. https://www.researchgate.net/figure/Schematic-of-DMD-process/set-up-with-simultaneous-wire-and-powder-feed_fig2_307629860(accessed Jun. 16, 2023).*

[48] *Powder Metallurgy: What Is It? Processes, Parts, Metals Used. (n.d.). https://www.iqsdirectory.com/articles/powder-metal-parts/powder-metallurgy.html(accessed Jun. 15, 2023).*

[49] *'L. Lü et al., Mechanical Alloying © Kluwer Academic Publishers 1(accessed May 29, 2023).*

[50] *Gorrasi, G. (2015). Mechanical milling as a technology to produce structural and functional bio-nanocomposites.*

[51] *Suryanarayana, C. (2007). Mechanical alloying and milling / C. Suryanarayana. ResearchGate.*

[52] *Fig. 11.1 a SPEX 8000 mixer/mill in the assembled condition. b A vial. . . (n.d.). ResearchGate. https://www.researchgate.net/figure/a-SPEX-8000-mixer-mill-in-the-assembled-condition-b-A-vial-and-balls_fig1_303097998 (accessed May 30, 2023).*

[53] *A. Llorente, B. Serrano, J. Baselga, G. Gedler, and R. Ozisik, (Feb. 2019)'Jet Milling as an Alternative Processing Technique for Preparing Polysulfone Hard Nanocomposites'.*

[54] *THURNE. (2022, March 7). Micronization Mill/ Spiral Jet mill - THURNE.*

[55] *c, A. S. (n.d.). CryoMill. ATS Scientific. https://ats/scientific.com/products/cryomill(accessed May 30, 2023).*

[56] *'Ball mill', Wikipedia. (Dec. 16, 2022). [Online]. Available: https://en.wikipedia.org/w/index.php?title=Ball_mill&oldid=1127717464*

[57] *Fig. 5. (a) Model 1-S attritor. (b) Arrangement of rotating arms on a. . . (n.d.). ResearchGate. https://www.researchgate.net/figure/a-Model-1-S-attritor-*

bArrangement-of-rotating-arms-on-a-shaft-in-the-attrition-ball_fig5_44564802 (accessed May 30, 2023).

[58] Joy, J., Krishnamoorthy, A., Tanna, A. R., Kamathe, V., Nagar, R., & Srinivasan, S. S. (2022). Recent Developments on the Synthesis of Nanocomposite Materials via Ball Milling Approach for Energy Storage Applications. Applied Sciences, 12(18), 9312.

[59] Suryanarayana, C. (2019). Mechanical Alloying: A Novel Technique to Synthesize Advanced Materials.

[60] Anand, K. J. S., Varghese, S., & Kurian, T. (2016). Aqueous Dispersions of Latex Compounding Ingredients by Wet Ball Milling: Effect of Ball Size and Milling Time on Dispersion Quality. Transactions of the Indian Institute of Metals, 70(6), 1593– 1600.

[61] Wikipedia contributors. (2023). Glovebox. Wikipedia. https://en.wikipedia.org/wiki/Glovebox

[62] Planetary Micro Mill Pulverisette 7 – Lavallab. (n.d.). https://lavallab.com/products/crushers/planetary-micro-mill/(accessed Jun. 16, 2023).

[63] 'Scanning Electron Microscope Working Principle – StudiousGuy'. https://studiousguy.com/scanning-electron-microscope-working-principle/(accessed Jun. 16, 2023).

[64] 'Scanning Electron Microscope Working Principle – StudiousGuy'. https://studiousguy.com/scanning-electron-microscope-working-principle/(accessed Jun. 17, 2023).

[65] S. Dhandapani,T. Rajmohan,K. Palanikumar &M. Charan.(2015). 'Synthesis and characterization of dual particle (MWCNT+B4C) reinforced sintered hybrid aluminum matrix composites'.

[66] Malvern Panalytical. (n.d.). X-ray Diffraction (XRD) - Overview. https://www.malvernpanalytical.com/en/products/technology/xray-analysis/x-ray-diffraction. (accessed Jun. 17, 2023).

[67] X-ray Diffraction : XRD | Techniques | Fields | Toray Research Center | TORAY. (n.d.). https://www.toray-research.co.jp/en/technicaldata/techniques/XRD.html (accessed Jun. 17, 2023).

[68] *Elsevier. (n.d.). Raviathul Basariya , V.C. Srivastava , N.K. Mukhopadhyay.(2014). Microstructural characteristics and mechanical properties of carbon nanotube reinforced aluminum alloy composites produced by ball milling.*

[69] *Gowda, A. C., Koppad, P. G., Sethuram, D., & Keshavamurthy, R. (2018). Morphology Studies on Mechanically Milled Aluminium Reinforced with B4C and CNTs.*

[70] *Essai des matériaux avec la méthode nanoindentation. (n.d.). Essai Des Matériaux Avec La Méthode Nanoindentation. https://www.helmut/fischer.com/fr/techniques/nanoindentation. (accessed Jun. 17, 2023).*

[71] *AZoNano.com. (2022, November 3). Carbon Nanotube Metal Matrix Composites. https://www.azonano.com/article.aspx?ArticleID=3149 (accessed Mar. 11, 2023).*

[72] *Wang, S., & Zhao, H. (2020). Low Temperature Nanoindentation: Development and Applications. Micromachines, 11(4), 407.*

[73] *Alizadeh, A. M., Abdollahi, A., & Biukani, H. (2015). Creep behavior and wear resistance of Al 5083 based hybrid composites reinforced with carbon nanotubes (CNTs) and boron carbide (B4C).*